Statistical Distribution of Quantum Entanglement for a Random Bipartite State

**Celine Nadal · Satya N. Majumdar ·
Massimo Vergassola**

Abstract We compute analytically the statistics of the Renyi and von Neumann entropies (standard measures of entanglement), for a random pure state in a large bipartite quantum system. The full probability distribution is computed by first mapping the problem to a random matrix model and then using a Coulomb gas method. We identify three different regimes in the entropy distribution, which correspond to two phase transitions in the associated Coulomb gas. The two critical points correspond to sudden changes in the shape of the Coulomb charge density: the appearance of an integrable singularity at the origin for the first critical point, and the detachment of the rightmost charge (largest eigenvalue) from the sea of the other charges at the second critical point. Analytical results are verified by Monte Carlo numerical simulations. A short account of part of these results appeared recently in Nadal et al. (Phys. Rev. Lett. 104:110501, 2010).

1 Introduction

Entanglement plays a crucial role in quantum information and computation as a measure of nonclassical correlations between parts of a quantum system [1]. The strength of those quantum correlations is significant in highly entangled states, which are involved and exploited in powerful communication and computational tasks that are not possible classically. Random pure states are of special interest as their average entropy is close to its possible maximum

C. Nadal (✉) · S.N. Majumdar
Univ. Paris Sud, CNRS, LPTMS, UMR 8626, Orsay 91405, France
e-mail: celine.nadal@u-psud.fr

S.N. Majumdar
e-mail: majumdar@lptms.u-psud.fr

M. Vergassola
Institut Pasteur, CNRS URA 2171, 75724 Paris 15, France
e-mail: massimo@pasteur.fr

value [2–4]. Taking a quantum state at random also corresponds to assuming minimal prior knowledge about the system [5]. Random states can thus be seen as "typical states" to which an arbitrary time-evolving quantum state may be compared. In addition, random states are useful in the context of quantum chaotic or nonintegrable systems [6–8].

There exist several measures for quantifying entanglement [9]. For a bipartite quantum system, the entropy (either the von Neumann or the Renyi entropies) is a well-known measure of entanglement. For a multipartite system, the full distribution of bipartite entanglement between two parts of the system has been proposed as a measure of multipartite entanglement [10, 11]. The distribution of entropy in a bipartite system is thus generally useful for characterizing entanglement properties of a random pure state.

Statistical properties of observables such as the von Neumann entropy, concurrence, purity or the minimum eigenvalue for random pure states have been studied extensively [2–4, 12–19]. In particular, the average von Neumann entropy is known to be close to its maximal value (for a large system). In contrast, few studies have addressed the full distribution of the entropy: only the distribution of the purity for very small systems [15] and partial information on the Laplace transform of the purity distribution for large systems [12] have previously appeared in the literature.

Our purpose here is to focus on the full distribution of the Renyi entropy for a random pure state in a large bipartite quantum system. Renyi entropy is defined as $S_q = \frac{1}{1-q} \ln \Sigma_q$ where $\Sigma_q = \sum_i \lambda_i^q$ and λ_i's are the eigenvalues of the reduced density matrix, the so called Schmidt coefficients. The parameter $1 \leq q < \infty$ characterizes different measures of entropy. In the limit $q \to 1$, it corresponds to the von Neumann entropy $S_{\mathrm{VN}} = -\sum_i \lambda_i \ln(\lambda_i)$, while for $q \to \infty$, it is given by $S_\infty = -\ln(\lambda_{\max})$. For $q = 2$, it reduces to $S_2 = -\ln(\Sigma_2)$ where $\Sigma_2 = \sum_i \lambda_i^2$ is the so called purity. In this paper, we compute analytically the probability distribution of the Renyi entropy S_q for arbitrary $q \in [1, \infty]$ for a random pure state. In particular, we show that the common idea that a random pure state is maximally entangled is not quite correct: while the average entropy is indeed close to its maximal value [2–4], the probability of an almost maximally entangled state is in fact vanishingly small. This statement requires to compute the full probability distribution of the entropy, namely its large deviation tails, which is one of the goals achieved in our paper.

The calculation of the Renyi entropies' distribution proceeds by mapping the entanglement problem to an equivalent random matrix model, which describes the statistical properties of the reduced density matrix of a subsystem. We can then use Coulomb gas methods borrowed from random matrix theory. We identify three regimes in the distribution of the entropy, as a direct consequence of two phase transitions in the associated Coulomb gas problem. One of those transitions is akin to a Bose-Einstein condensation, with one charge of the Coulomb gas detaching from the sea of the other charges—or equivalently one eigenvalue of the reduced density matrix becoming much larger than the others.

This paper is a detailed version of a short letter that was published recently [20]. It thus contains all explicit formulas for our results and details about analytical proofs and numerical simulations that we could not provide in [20] for lack of space. Furthermore, this paper also contains new results, especially for the third regime of the distribution (see below), the von Neumann entropy and the maximal eigenvalue of the density matrix.

We note that shortly after our letter [20], another article was published [21], which is independent and concentrates on the special case of purity, i.e. the case $q = 2$ of the Renyi entropy. Results for $q = 2$ that appear both in [21] and in [20] and here, are in agreement. Conversely, the nature of the singularities for the distribution itself (considered in [20] and here) and its Laplace transform (considered in [21] as well as in previous work [12]) is different, thus providing complementary information. Furthermore, in [20] and here, we provide detailed numerical simulations for $q = 2$ to test and confirm analytical results. Finally,

we emphasize that our results, presented below, hold for all $q \in [1, \infty]$ and that the limiting cases $q \to 1$ (von Neumann entropy) and $q \to \infty$ (the distribution of the maximum Schmidt coefficient) are particularly relevant for the physical problem of quantum entanglement.

The plan of the paper is as follows. In Sect. 2, we describe precisely our model of bipartite quantum system for the direct product $\mathcal{H}_A \otimes \mathcal{H}_B$ of two Hilbert spaces $\mathcal{H}_A$ and $\mathcal{H}_B$. In Sect. 3, we analyze the distribution of the eigenvalues λ_i of the reduced density matrices of the two subsystems. In particular, we compute the average density of eigenvalues and explain the Coulomb gas method that we also use later for computing the distribution of the Renyi entropy $S_q = \frac{1}{1-q} \ln \Sigma_q$ where $\Sigma_q = \sum_i \lambda_i^q$. In Sect. 4, we compute the full distribution of Σ_q for a large system. We find two phase transitions in the associated Coulomb gas, and thus three regimes for the distribution of Σ_q. In Sect. 5, using results from Sect. 4, we derive the distribution of the Renyi entropy S_q as well as the distribution of the von Neumann entropy (case $q \to 1$) and the distribution of the largest eigenvalue ($q \to \infty$). Finally in Sect. 6, we present results obtained by Monte Carlo numerical simulations that we performed to test and verify our analytical predictions.

2 Random Bipartite State

In this section, we set the problem of bipartite entanglement for a random pure state. We first describe a bipartite quantum system, introduce then measures of entanglement (the von Neumann and Renyi entropies) and give finally the precise definition of random pure states.

2.1 Entanglement in a Bipartite Quantum System

Let us consider a bipartite quantum system $A \otimes B$ composed of two subsystems A and B of respective dimensions N and M. The system is described by the product Hilbert space $\mathcal{H}_{AB} = \mathcal{H}_A \otimes \mathcal{H}_B$ with $N = \dim(\mathcal{H}_A)$ and $M = \dim(\mathcal{H}_B)$. Here, we shall be interested in the limit where N and M are large and $c = \frac{N}{M}$ is fixed. We shall take $N \leq M$, i.e. $c \leq 1$, so that A and B play the role of the subsystem of interest and of the environment, respectively.

Let $|\psi\rangle$ be a pure state of the full system. Its density matrix $\rho = |\psi\rangle\langle\psi|$ is a positive semi-definite Hermitian matrix normalized as $\mathrm{Tr}\,\rho = \langle\psi|\psi\rangle = 1$. The density matrix can thus be diagonalized, its eigenvalues are non-negative and their sum is unity. Subsystem A is described by its reduced density matrix $\rho_A = \mathrm{Tr}_B[\rho] = \sum_{\alpha^B=1}^{M} \langle\alpha^B|\rho|\alpha^B\rangle$, where $|\alpha^B\rangle$ is an orthonormal basis of $\mathcal{H}_B$. Similarly, B is described by $\rho_B = \mathrm{Tr}_A[\rho]$. It is easy to show that the reduced matrices ρ_A and ρ_B share the same set of non-negative eigenvalues $\{\lambda_1, \ldots, \lambda_N\}$ with $\sum_{i=1}^{N} \lambda_i = 1$.

Any pure state can be written as $|\psi\rangle = \sum_{i=1}^{N} \sum_{\alpha=1}^{M} x_{i,\alpha} |i^A\rangle \otimes |\alpha^B\rangle$ where $|i^A\rangle \otimes |\alpha^B\rangle$ is a fixed orthonormal basis of $\mathcal{H}_{AB}$. The singular value decomposition of the matrix $x_{i,\alpha}$ permits to recast the previous expression in the so-called Schmidt decomposition form:

$$|\psi\rangle = \sum_{i=1}^{N} \sqrt{\lambda_i} |m_i^A\rangle \otimes |\mu_i^B\rangle \tag{1}$$

where $|m_i^A\rangle$ and $|\mu_i^B\rangle$ represent the eigenvectors of ρ_A and ρ_B, respectively, associated with the same eigenvalue λ_i.

The representation (1), namely the Schmidt number n_S of strictly positive eigenvalues, is very useful for characterizing the entanglement between subsystems A and B. For example, let us consider two limiting cases:

(i) If only one of the eigenvalues, say λ_i, is non zero then $\lambda_i = 1$, $n_S = 1$ and the state of the full system $|\psi\rangle = |m_i^A\rangle \otimes |\mu_i^B\rangle$ is a product state, which is said to be separable. The system is unentangled.

(ii) If all the eigenvalues are equal ($\lambda_j = 1/N$ for all j), $n_S = N$ and $|\psi\rangle$ is a superposition of all product states. The system is maximally entangled.

A standard measure of entanglement between two subsystems A and B is the von Neumann entropy of either subsystem: $S_{\text{VN}} = -\text{Tr}[\rho_A \ln \rho_A] = -\sum_{i=1}^{N} \lambda_i \ln \lambda_i$, which reaches its minimum 0 when the system is unentangled (situation (i) above) and its maximum $\ln N$ when the system is maximally entangled (situation (ii)). Another useful measure of entanglement is the Renyi entropy of order q (for $q > 0$):

$$S_q = \frac{1}{1-q} \ln \left[\sum_{i=1}^{N} \lambda_i^q \right], \tag{2}$$

which also reaches its minimal value 0 in situation (i) and its maximal value $\ln N$ in situation (ii). As one varies the parameter q, the Renyi entropy interpolates between the von Neumann entropy ($q \to 1^+$) and $-\ln \lambda_{\max}$ ($q \to \infty$) where $\lambda_{\max}$ is the largest eigenvalue of the reduced density matrices.

2.2 Random Pure States

A pure state is called random when it is sampled according to the uniform Haar measure, which is unitarily invariant. Specifically, a random pure state is defined as $|\psi\rangle = \sum_{i=1}^{N} \sum_{\alpha=1}^{M} x_{i,\alpha} |i^A\rangle \otimes |\alpha^B\rangle$, where $|i^A\rangle \otimes |\alpha^B\rangle$ is a fixed orthonormal basis of $\mathcal{H}_{AB}$ and where the variables $\{x_{i,\alpha}\}$ are uniformly distributed among the sets of $\{x_{i,\alpha}\}$ satisfying the constraint $\sum_{i,\alpha} |x_{i,\alpha}|^2 = 1$ (normalization of $|\psi\rangle$). Equivalently, the probability density function (pdf) of the $N \times M$ matrix X with entries $x_{i,\alpha}$ can be written

$$P(X) \propto \delta(\text{Tr}(XX^\dagger) - 1) \propto e^{-\frac{\beta}{2}\text{Tr}(XX^\dagger)} \delta(\text{Tr}(XX^\dagger) - 1), \tag{3}$$

with the second equality showing that the pdf can also be seen as a Gaussian supplemented by the unit-trace constraint.

In the basis $|i^A\rangle$ of $\mathcal{H}_A$, the reduced density matrix of subsystem $\mathcal{A}$ is simply given by $\rho_A = XX^\dagger$. In general, when X is a $N \times M$ Gaussian random matrix, i.e. $P(X) \propto e^{-\frac{\beta}{2}\text{Tr}(XX^\dagger)}$ (iid Gaussian entries $x_{i,\alpha}$ that are real for a Dyson index $\beta = 1$, complex for $\beta = 2$), the $N \times N$ matrix $XX^\dagger$ is a Wishart matrix whose distribution of eigenvalues is [22]:

$$P_{Wishart}(\lambda_1, \ldots, \lambda_N) \propto e^{-\frac{\beta}{2}\sum_i \lambda_i} \prod_{i=1}^{N} \lambda_i^{\frac{\beta}{2}(M-N+1)-1} \prod_{i<j} |\lambda_i - \lambda_j|^\beta. \tag{4}$$

The Vandermonde determinant $\prod_{i<j} |\lambda_i - \lambda_j|^\beta$ makes that the eigenvalues are strongly correlated and they physically tend to repel each other.

The major difference between the matrix $\rho_A = XX^\dagger$ in the quantum problem and a standard Wishart matrix stems from the unit trace constraint $\text{Tr}[\rho_A] = 1$. The constraint is to be included in the distribution of the eigenvalues of ρ_A, which is given [4, 13] by:

$$P(\lambda_1, \ldots, \lambda_N) = B_{M,N} \, \delta\left(\sum_i \lambda_i - 1\right) \prod_{i=1}^{N} \lambda_i^{\frac{\beta}{2}(M-N+1)-1} \prod_{i<j} |\lambda_i - \lambda_j|^\beta, \tag{5}$$

with $\beta = 2$ (the $x_{i,\alpha}$ are complex) and the normalization constant $B_{M,N}$ computed using Selberg's integrals [13]:

$$B_{M,N} = \frac{\Gamma(MN\beta/2)\,\Gamma(1+\beta/2)^N}{\prod_{j=0}^{N-1}\Gamma((M-j)\beta/2)\,\Gamma(1+(N-j)\beta/2)}. \tag{6}$$

The presence of a fixed trace constraint (as in (5)) is known to have important consequences on the spectral properties of a matrix [23–25]. We will see that in the present context also, the fixed trace constraint does play an important and crucial role. In particular, this constraint is directly responsible for a Bose-Einstein type condensation transition that will be discussed in the context of the probability distribution of the entanglement entropy.

Since the eigenvalues λ_i of ρ_A are random variables for a random pure state, any observable is a random variable as well. Statistical properties of observables, namely of various measures of entanglement such as the von Neumann entropy [4, 26–28], G-concurrence [14], purity [12, 15] or minimum eigenvalue [16–19], have been studied extensively. In particular, Page [4] computed the average von Neumann entropy in the limit $M \geq N \gg 1$: $\langle S_{VN} \rangle \approx \ln N - \frac{N}{2M}$. He also conjectured its value for finite N and M (which was proved later [26–28]). In contrast, there have been few studies on the full distribution of the entropy, except for the purity $\Sigma_2 = \sum_i \lambda_i^2$ whose distribution is known exactly for small N (2, 3 and 4) [15]. For large N, the Laplace transform of the purity distribution (generating function of the cumulants) was studied recently [12] for positive values of the Laplace variable. However, when inverted, the previous quantity provides only partial information about the purity distribution.

Here, we compute analytically the full distribution of the Renyi entropy S_q (defined in (2)) or equivalently of $\Sigma_q = \sum_{i=1}^N \lambda_i^q = \exp[(1-q)S_q]$, for large N. As for the von Neumann entropy, the average value of the Renyi entropies is close to their maximal value $\ln N$ (maximal entanglement): $\langle S_q \rangle \approx \ln N - \bar{z}(q)$, where $\bar{z}(q) > 0$ (for $q > 0$) is independent of N for large N. For example, for $M \approx N$ and $q = 2$, we have $\bar{z}(q = 2) = \ln 2$. However, we show below that the probability that S_q approaches its maximal value $\ln N$ is again very small.

3 Distribution of the Eigenvalues of ρ_A

The eigenvalues of the reduced density matrix ρ_A are distributed according to the law in (5). Given this joint distribution, the first natural object to study is the average spectral density $\rho_{N,M}(\lambda) = \frac{1}{N}\sum_{i=1}^N \langle \delta(\lambda - \lambda_i)\rangle$. This average density $\rho_{N,M}(\lambda)d\lambda$ also gives the probability to find an eigenvalue between λ and $\lambda + d\lambda$ (the one-point marginal of the joint distribution). For finite (N, M), this average density was computed first for $\beta = 2$ [29, 30] and very recently for $\beta = 1$ [31]. However, these formulae involve rather complicated special functions and taking the asymptotic large N, large M limit is nontrivial. Here we take a complementary route which is well suited to derive exactly the asymptotic limit. We take the limit $N \to \infty$, $M \to \infty$ but keeping their ratio $0 \leq c = N/M \leq 1$ fixed. For the spectral density, we henceforth use a shorthand notation $\rho_N(\lambda) = \rho_{N,N/c}(\lambda)$. We obtain easily via a Coulomb gas approach the limiting form of $\rho_N(\lambda)$ for large N.

Due to the unit trace constraint $\sum_{i=1}^N \lambda_i = 1$, the typical amplitude of the eigenvalues is $\lambda_{typ} \sim \frac{1}{N}$ for large N. Since $\lambda_{typ} \sim \frac{1}{N}$ (and ρ_N is normalized to unity), we expect (as will be proved below) that the average density for large N has a scaling form:

$$\rho_N(\lambda) \approx N\,\rho^*(\lambda N). \tag{7}$$
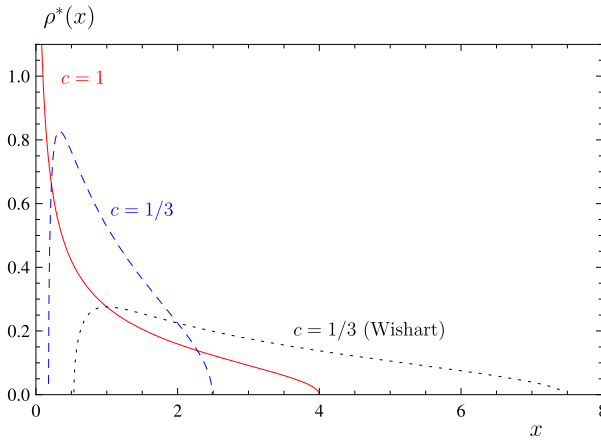
Fig. 1 (Color online) The rescaled average density $\rho^*(x)$ of the eigenvalues for the density matrix of a quantum subsystem. The rescaled density is defined by $\rho_N(\lambda) \approx N \, \rho^*(\lambda N)$ for large N (see (8)) and is plotted for $c = \frac{N}{M} = 1$ (*red solid line*) and $c = 1/3$ (*blue dashed line*). The density is compared with the rescaled average density of Wishart eigenvalues (random matrix theory): $\rho_W^*(x)$ defined by $\rho_N^W(\lambda) \approx \frac{1}{N} \, \rho_W^*(\frac{\lambda}{N})$ (see (10)) plotted for $c = \frac{N}{M} = 1$ (*red solid line*) and $c = 1/3$ (*black dotted line*). The different dependencies on c for $\rho^*(x)$ and $\rho_W^*(x)$ make that, even after their different rescaling in N, the two distributions are equal only for $c = 1$

Using the Coulomb gas method (explained in Sect. 4.1), we find an exact expression for the rescaled density $\rho^*(x)$:

$$\rho^*(x) = \frac{1}{2\pi c x} \sqrt{x - L_1} \, \sqrt{L_2 - x} \,, \tag{8}$$

where the right and left edges read $L_2 = c(\sqrt{\frac{1}{c}} + 1)^2$, $L_1 = c(\sqrt{\frac{1}{c}} - 1)^2$ and we recall that $c = N/M \leq 1$.

For $c = 1$ ($N \approx M$), $L_1 = 0$, $L_2 = 4$ and the rescaled density reduces to:

$$\rho^*(x) = \frac{1}{2\pi} \sqrt{\frac{4 - x}{x}} \,. \tag{9}$$

On the other hand, for Wishart matrices (same distribution of eigenvalues but without the constraint $\sum_i \lambda_i = 1$), it is known that the average density of the eigenvalues is given, for large N and fixed $c = N/M$, by the Marčenko-Pastur law [46]:

$$\rho_N^W(\lambda) \approx \frac{1}{N} \, \rho_W^*\left(\frac{\lambda}{N}\right) \quad \text{with } \rho_W^*(x) = \frac{1}{2\pi x} \sqrt{x - L_1^W} \, \sqrt{L_2^W - x} \,, \tag{10}$$

with the right and left edges given by $L_2^W = (1 + \sqrt{\frac{1}{c}})^2$ and $L_1^W = (1 - \sqrt{\frac{1}{c}})^2$.

As expected, the scaling with N is different: $\lambda_{typ}^W \sim N$ for a Wishart eigenvalue, whereas the unit trace constraint makes that $\lambda_{typ} \sim 1/N$ for an eigenvalue of the quantum density matrix ρ_A.

For $c = 1$, the two edges $L_1^W = 0$, $L_2^W = 4$ and $\rho_W^*(x) = \rho^*(x)$. However, for a general $c < 1$ the rescaled densities are not quite the same (even though they have the same shape):
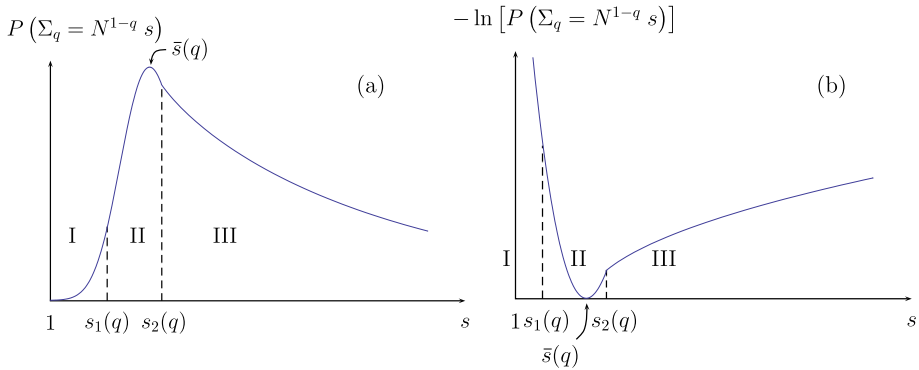
Fig. 2 Schematic distribution of $\Sigma_q = \sum_i \lambda_i^q = N^{1-q} s$ as a function of s for (very) large N. Panel (**a**) shows the shape of the pdf of Σ_q, while (**b**) shows the shape of the rate function $-\ln P(\Sigma_q = N^{1-q}s)$. Two critical points $s_1(q)$ and $s_2(q)$ separate three regimes **I**, **II** and **III**, characterized by the different optimal densities shown in Fig. 3. The maximally entangled state $s = 1$ is at the extreme-left of the distribution, well spaced from the mean value $\bar{s}(q)$

$\rho_W^*(x) = c \, \rho^*(xc)$. In Fig. 1, plots of the rescaled density $\rho^*(x)$ and comparisons to the shape of the rescaled density for a standard Wishart matrix $\rho_W^*(x)$ are shown for $c = 1$ and $c = 1/3$.

4 Distribution of $\Sigma_q = \sum_i \lambda_i^q$ for $q > 1$ and $c = 1$

This section is somewhat long as it contains the bulk of the details of our calculations. Hence it is useful to start with a summary of the main results obtained in Sects. 4.1–4.3 as well as the main picture that emerges out of these calculations.

In this section, we compute the full distribution of $\Sigma_q = \sum_i \lambda_i^q$, and thus of the Renyi entropy $S_q = \ln(\Sigma_q)/(1 - q)$ for large N. We take for simplicity $M \approx N$, i.e. $c = 1$, but our method can be easily extended to $c < 1$ as well. For simplicity, we will also restrict ourselves to the case $q \geq 1$. However, our method is also easily extendable to the case $0 < q < 1$. Since $\sum_i \lambda_i = 1$ and $x \to x^q$ is convex for $q > 1$, we have $N^{1-q} \leq \Sigma_q \leq 1$ (or equivalently $\ln N \geq S_q \geq 0$). The lower bound $\Sigma_q = N^{1-q}$ corresponds to the maximally entangled case (situation (ii) in Sect. 2.1), when $\lambda_j = 1/N$ for all j: the entropy is $S_q = \ln N$. The upper bound $\Sigma_q = 1$ corresponds to the unentangled case (situation (i) in Sect. 2.1) when only one of the λ_i is non zero (and thus equal to one): the entropy is zero.

The scaling $\lambda_{typ} \sim 1/N$ implies that $\Sigma_q \sim N^{1-q}$ for large N. Let $s \equiv \Sigma_q N^{q-1}$ be the rescaled variable $s \sim O(1)$. In Fig. 2, a typical plot of the probability density function (pdf) $P(\Sigma_q = N^{1-q} s)$ is shown: the distribution has a Gaussian peak (centered on the mean value $s = \bar{s}(q)$) flanked on both sides by non-Gaussian tails. We show below that there are two critical values $s = s_1(q)$ and $s = s_2(q)$ separating three regimes **I** ($1 \leq s < s_1(q)$), **II** ($s_1(q) < s < s_2(q)$) and **III** ($s_2(q) < s$).

At the first critical point $s_1(q)$, the distribution has a weak singularity (discontinuity of the third derivative). At the second critical point $s_2(q)$, a Bose-Einstein type condensation transition occurs and the distribution changes shape abruptly; the first derivative is discontinuous in the limit $N \to +\infty$, this means that this transition is actually a first-order phase transition. The schematic plot of the distribution of Σ_q (for large N) in Fig. 2 clearly shows
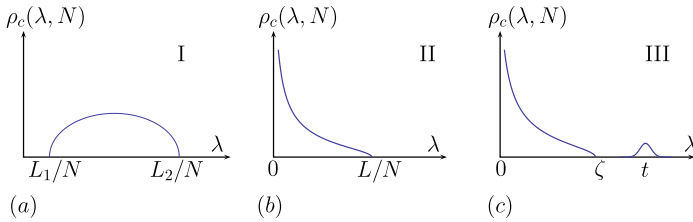
Fig. 3 Scheme of the optimal saddle point density ρ_c of the eigenvalues (or, equivalently, of the Coulomb gas of charges) for (**a**) $1 \leq s < s_1(q)$ (regime **I**), (**b**) $s_1(q) < s < s_2(q)$ (regime **II**) and (**c**) $s > s_2(q)$ (regime **III**). In regime **III**, the maximal eigenvalue $\lambda_{\max} = t$ becomes much larger than the other eigenvalues, as shown by the isolated bump in (**c**)
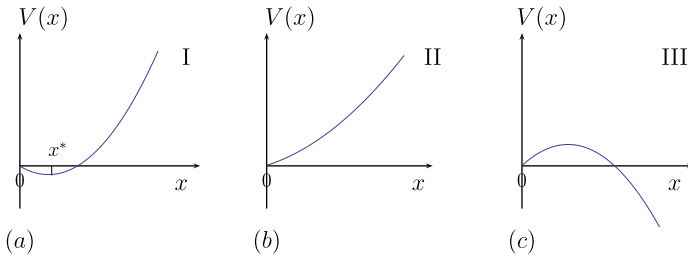
Fig. 4 Scheme of the effective potential $V(x)$ seen by the charges of the Coulomb gas (eigenvalues) for (**a**) $1 \leq s < s_1(q)$ (regime **I**), (**b**) $s_1(q) < s < s_2(q)$ (regime **II**) and (**c**) $s > s_2(q)$ (regime **III**). In regimes **I** and **II**, the charges are confined close to the minimum of the effective potential. In regime **III**, the potential is not anymore bounded from below. Therefore, one charge detaches from the sea of the other charges: the maximal eigenvalue becomes much larger than the other

the three regimes **I**, **II** and **III** and the discontinuity of the derivative at $s = s_2$ (transition between **II** and **III**). These changes are a direct consequence of two phase transitions in the associated Coulomb gas problem, more precisely in the shape of the optimal charge density. Figures 4 and 3 show respectively the effective potential seen by the charges and the density of charges in the three regimes. In particular, in regime **III**, the potential is not anymore bounded from below, one charge detaches from the sea of the other charges.

More precisely, the probability density function of Σ_q for large N and $q > 1$ displays three different regimes:

$$P(\Sigma_q = N^{1-q} s) \approx \begin{cases} \exp\{-\beta N^2 \Phi_I(s)\} & \text{for } 1 \leq s < s_1(q)\,; \\ \exp\{-\beta N^2 \Phi_{II}(s)\} & \text{for } s_1(q) < s < s_2(q)\,; \\ \exp\{-\beta N^{1+\frac{1}{q}} \Psi_{III}(s)\} & \text{for } s > s_2(q)\,. \end{cases} \quad (11)$$

The exact mathematical meaning of the "$\approx$" sign is a logarithmic equivalence: $-\frac{\ln P(\Sigma_q = N^{1-q} s)}{\beta N^2} \to \Phi_I(s)$ as $N \to \infty$ with fixed $s \in [1, s_1(q)[$ (resp. Φ_{II} for fixed $s \in]s_1(q), s_2(q)[$) and $-\frac{\ln P(\Sigma_q = N^{1-q} s)}{\beta N^{1+1/q}} \to \Psi_{III}(s)$ as $N \to \infty$ with fixed $s > s_2(q)$. The rate functions Φ_I, Φ_{II} and Ψ_{III} (as well as s_1 and s_2) are independent of N—but they depend on the parameter q. Explicit expressions of the functions Φ_I and Φ_{II} are given in (32) and (36) for $q = 2$, and in (41) for a general $q > 1$; an explicit expression of Ψ_{III} is given in (44) for a general $q > 1$ (and in (45) for $q = 2$). As shown in Figs. 5 and 6 (resp. for

$N = 50$ and $N = 1000$), we also did some Monte Carlo simulations (as explained in Sect. 6) and found that our analytical predictions agree very well with the numerical data.

Regime **II** includes the mean value $\langle \Sigma_q \rangle \approx N^{1-q} \bar{s}(q)$, i.e. $s_1(q) < \bar{s}(q) \leq s_2(q)$ for every q. The mean value is explicitely given by:

$$\langle \Sigma_q \rangle \approx N^{1-q} \bar{s}(q) \quad \text{with } \bar{s}(q) = \frac{\Gamma(q + 1/2)}{\sqrt{\pi} \Gamma(q + 2)} 4^q . \tag{12}$$

For large N, the distribution of Σ_q given in (11) is highly peaked around its average (because of the factor N^2 in regime **II**): the average value of Σ_q coincides then with the most probable value, i.e. $\bar{s}(q)$ is the minimum of $\Phi_{II}(s)$. The quadratic behaviour of $\Phi_{II}(s)$ around this minimum gives the Gaussian behaviour of the distribution of Σ_q around its average (and thus gives the variance of Σ_q). We get:

$$P(\Sigma_q = N^{1-q} s) \approx \exp\left\{ -\beta N^2 \frac{(s - \bar{s}(q))^2}{2\sigma_q^2} \right\} \quad \text{for } s \text{ close to } \bar{s}(q). \tag{13}$$

Therefore, the variance of Σ_q is given by:

$$\text{Var } \Sigma_q = \langle \Sigma_q^2 \rangle - \langle \Sigma_q \rangle^2 \approx \frac{\sigma_q^2}{\beta N^{2q}} \quad \text{with } \sigma_q^2 = \frac{4^{2q}}{2\pi} q(q-1)^2 \frac{\Gamma(q+1/2)^2}{\Gamma(q+2)^2}. \tag{14}$$

The distribution has a Gaussian peak flanked by non-Gaussian tails described by the rate functions Φ_I (left tail) and Ψ_{III} (right tail). Conversely, the rate function Φ_{II} describes the middle part of the distribution, which includes the Gaussian behaviour in the neighbourhood of the average.

In the limit $N \to \infty$, $s_1(q)$ and $s_2(q)$ do not depend on N and the second critical value $s_2(q)$ is actually equal to the mean value $\bar{s}(q)$ of s:

$$s_1(q) = \frac{\Gamma(q+3/2)}{\sqrt{\pi} \Gamma(q+2)} \left(\frac{4(q+1)}{3q} \right)^q \quad \text{and} \quad s_2(q) = \bar{s}(q) = \frac{\Gamma(q+1/2)}{\sqrt{\pi} \Gamma(q+2)} 4^q . \tag{15}$$

However, for a large but finite N, $s_2(q, N)$ actually depends on N and is given in (16) below.

The convergence in N for the regimes **I** and **II** is very fast: the agreement between numerical simulations and analytical predictions in the limit $N \to \infty$ is very good already for $N \simeq 50$. However, the second transition, between regime **II** and **III**, is affected by finite-size effects, that remain important even for $N \simeq O(10^3)$. Their main effect is a shift in the value of the critical point s_2. The transition actually occurs at a value $s_2(q, N)$ that depends on N, is a bit larger than $\bar{s}(q)$ and tends slowly to $\bar{s}(q)$ as $N \to \infty$. More precisely, the second transition occurs at $s = s_2(q, N)$ with

$$s_2(q, N) \approx \bar{s}(q) + \frac{[\sqrt{q/2} (q-1) \bar{s}(q)]^{2q/(2q-1)}}{N^{(q-1)/(2q-1)}} \quad \text{for large but finite } N. \tag{16}$$

For example, for $q = 2$, we have $\bar{s}(q = 2) = 2$ and $s_2(q = 2, N) \approx 2 + \frac{2^{4/3}}{N^{1/3}} - \frac{2^{5/3} \ln N}{3N^{2/3}}$ for large but finite N.

The extreme left of the distribution corresponds to maximally entangled states: $s \to 1^+$ means that $\sum_i \lambda_i^q = \Sigma_q \to N^{1-q}$, that is the case where all the eigenvalues are equal and the state is maximally entangled (situation (ii)). As $s \to 1$, $\Phi_I(s)$ tends to $+\infty$, thus the pdf $P(\Sigma_q = N^{1-q} s)$ tends rapidly towards zero. For example, for $q = 2$, we have $P(\Sigma_q =$

$N^{1-q}s) \approx (s-1)^{\beta N^2/4}$ as $s \to 1^+$. This implies that the probability of a maximally entangled configuration is very small (for large N).

Similarly, the extreme right $s \to +\infty$ of the distribution corresponds to weakly entangled states. An unentangled state has indeed only one non-zero eigenvalue, λ_i, thus $S = \Sigma_q = 1$ (situation (i)). We can actually compute the expression of the pdf for the scaling $\Sigma_q = S$ with $S \approx O(1)$ ($S \gg s/N$) and $0 < S < 1$. For $q = 2$, we get: $P(\Sigma_2 = S) \approx (1 - \sqrt{S})^{\beta N^2/2}$ for $N \to \infty$ with $S \approx O(1)$. For $S \to 1^-$, the pdf of Σ_q is again tending very rapidly towards zero: unentangled states are highly unlikely.

4.1 Computation of the pdf of Σ_q: Associated Coulomb Gas

In this subsection, we explain how we compute the pdf (probability density function) of Σ_q using a Coulomb gas method.

The mapping from random matrix eigenvalues to a Coulomb gas problem is well-known in random matrix theory [32] and has been recently used in a variety of contexts that include the distribution of the extreme eigenvalues of Gaussian and Wishart matrices [33–37], purity partition function in bipartite systems [12], nonintersecting Brownian interfaces [38], quantum transport in chaotic cavities [39, 40], information and communication systems [41], and the index distribution for Gaussian random fields [42, 43] and Gaussian matrices [44]. Here, we use similar methods yet the problem is quite different due to the constraint $\sum_i \lambda_i = 1$. First, the scaling with N (for large N) differs from standard Wishart matrices. Indeed, $\lambda_{typ} \sim 1/N$ in our problem of entanglement whereas $\lambda_{typ}^W \sim N$ for a Wishart matrix. However, the effect of the constraint $\sum_i \lambda_i = 1$ is not just the rescaling of standard Wishart results by a factor of $1/N^2$ as it may seem. It turns out that the constraint has more serious consequences and leads to fundamentally different and new behavior (including a condensation transition which is absent in Wishart matrices) that we will demonstrate.

The pdf of Σ_q is by definition:

$$P(\Sigma_q, N) = \int P(\lambda_1, \dots, \lambda_N) \, \delta\left(\sum_i \lambda_i^q - \Sigma_q\right)\left(\prod_i d\lambda_i\right). \tag{17}$$

The joint pdf of the eigenvalues $P(\lambda_1, \dots, \lambda_N)$ is given in (5) and can be seen as a Boltzmann weight at inverse temperature β:

$$P(\lambda_1, \dots, \lambda_N) \propto \exp\{-\beta E[\{\lambda_i\}]\}, \tag{18}$$

where the energy $E[\{\lambda_i\}] = -\gamma \sum_{i=1}^N \ln \lambda_i - \sum_{i<j} \ln |\lambda_i - \lambda_j|$ (with $\sum_i \lambda_i = 1$) is the effective energy of a 2D Coulomb gas of charges: the charges repel each other electrostatically (logarithmic interaction in 2D). For large N, the effective energy is of order $E \sim O(N^2)$ (because of the logarithmic interaction potential). We can thus compute the multiple integral in (17) via the method of steepest descent: for large N, the configuration of $\{\lambda_i\}$ which dominates the integral is the one that minimizes the effective energy.

For (17) we also have to take into account the constraint $\sum_i \lambda_i^q = \Sigma_q$ (delta function in (17)). This will be done by adding in the effective energy a term $\mu_2'(\sum_i \lambda_i^q - \Sigma_q)$ where μ_2' plays the role of a Lagrange multiplier. Physically, this corresponds to adding an external potential $\mu_2' \lambda^q$ for the charges.

For large N, the eigenvalues are expected to be close to each other and the saddle point will be highly peaked, i.e. the most probable value and the mean coincide. We will thus assume that we can label the λ_i by a continuous average density of states $\rho(\lambda, N) =$

$N^{-1}\sum_i \langle \delta(\lambda - \lambda_i)\rangle = N\,\rho(x)$ with $\rho(x) = N^{-1}\sum_i \langle \delta(x - \lambda_i N)\rangle$ and $x = \lambda N$. However, we will see that this assumption is not correct for large Σ_q (large s): in the regime **III**, the maximal eigenvalue becomes much larger than the other eigenvalues. The maximal eigenvalue should then be treated on its own and be distinguished from the continuous average density.

Let us begin with the case where the eigenvalues can be described by the density $\rho(x)$. Then the pdf of Σ_q can be written as:

$$P(\Sigma_q = N^{1-q}\,s,\,N) \propto \int \mathcal{D}[\rho]\,\exp\{-\beta N^2\,E_s[\rho]\}\,, \qquad (19)$$

where the effective energy $E_s[\rho]$ is given by

$$E_s[\rho] = -\frac{1}{2}\int_0^\infty\int_0^\infty dx\,dx'\,\rho(x)\rho(x')\,\ln|x - x'| + \mu_0\left(\int_0^\infty dx\,\rho(x) - 1\right)$$
$$+ \mu_1\left(\int_0^\infty dx\,x\,\rho(x) - 1\right) + \mu_2\left(\int_0^\infty dx\,x^q\,\rho(x) - s\right). \qquad (20)$$

The Lagrange multipliers μ_0, μ_1 and μ_2 enforce respectively the constraints $\int \rho = 1$ (normalization of the density), $\sum_i \lambda_i = 1$ (unit trace) and $\sum_i \lambda_i^q = N^{1-q}\,s$ (delta function in (17)).

For large N, the method of steepest descent gives:

$$P(\Sigma_q = N^{1-q}\,s,\,N) \propto \exp\{-\beta N^2 E_s[\rho_c]\}\,, \qquad (21)$$

where ρ_c minimizes the energy (saddle point):

$$\left.\frac{\delta E_s}{\delta \rho}\right|_{\rho = \rho_c} = 0\,. \qquad (22)$$

The saddle point equation reads:

$$\int_0^\infty dx'\,\rho_c(x')\,\ln|x - x'| = \mu_0 + \mu_1 x + \mu_2 x^q \equiv V(x)\,, \qquad (23)$$

with $V(x)$ acting as an effective external potential. Differentiating with respect to x gives:

$$\mathcal{P}\int_0^\infty dx'\,\frac{\rho_c(x')}{x - x'} = \mu_1 + q\,\mu_2 x^{q-1} = V'(x)\,, \qquad (24)$$

where $\mathcal{P}$ denotes the Cauchy principal value. This singular integral equation can be solved by using a theorem due to Tricomi [45] that states that if the solution ρ^* has a finite support $[L_1, L_2]$, then the finite Hilbert transform defined by the equation $F(x) = \mathcal{P}\int_{L_1}^{L_2} dx'\,\frac{\rho^*(x')}{x - x'}$ can be inverted as

$$\rho^*(x) = \frac{1}{\pi\sqrt{x - L_1}\sqrt{L_2 - x}}\left[C - \mathcal{P}\int_{L_1}^{L_2}\frac{dx'}{\pi}\frac{\sqrt{x' - L_1}\sqrt{L_2 - x'}}{x - x'}F(x')\right], \qquad (25)$$

where the constant C fixes the integral of ρ^* via $\int_{L_1}^{L_2} dx\,\rho^*(x) = C$. We thus obtain a finite support density ρ_c which yields the answer for the regimes **I** and **II**.

In these regimes, the pdf of Σ_q is thus given by $P(\Sigma_q = N^{1-q} s, N) \approx \exp\{-\beta N^2 \Phi(s)\}$ where the rate function $\Phi(s)$ is equal to $E_s[\rho_c]$ up to an additive constant. More precisely, the normalized pdf reads:

$$P(\Sigma_q = N^{1-q} s, N) \approx \frac{\int \mathcal{D}[\rho] \exp\{-\beta N^2 E_s[\rho]\}}{\int \mathcal{D}[\rho] \exp\{-\beta N^2 E[\rho]\}}, \tag{26}$$

where $E_s[\rho]$ is given in (20) and $E[\rho]$ is the effective energy associated to the joint distribution of the eigenvalues (without further constraint, with $\mu_2 = 0$). The steepest descent for both the numerator and denominator gives:

$$P(\Sigma_q = N^{1-q} s, N) \approx \frac{\exp\{-\beta N^2 E_s[\rho_c]\}}{\exp\{-\beta N^2 E[\rho^*]\}} \approx \exp\{-\beta N^2 \Phi(s)\}, \tag{27}$$

with $\Phi(s) = E_s[\rho_c] - E[\rho^*]$ and where ρ^* (resp. ρ_c) is the density that minimizes $E[\rho]$ (resp. $E_s[\rho]$). The density $\rho^*(x)$ is thus simply the rescaled average density of states given in (9) (for $c = 1$). Finally, we get

$$\Phi(s) = E_s[\rho_c] - E[\rho^*] = E_s[\rho_c] - 1/4. \tag{28}$$

4.2 Regime **I** and **II**

Regimes **I** and **II** correspond to the case where the eigenvalues can be described by a continuous density $\rho(x)$, as explained above. In this case, we have seen that the pdf of Σ_q is given for large N by $P(\Sigma_q = N^{1-q} s, N) \approx \exp\{-\beta N^2 \Phi(s)\}$. In this section, we derive an explicit expression for $\Phi(s) = \Phi_I(s)$ in regime **I** i.e. for $1 \leq s < s_1(q)$ ((32) in Sect. 4.2.1 for $q = 2$) and $\Phi(s) = \Phi_{II}(s)$ in regime **II** i.e. for $s_1(q) < s < s_2(q)$ ((36) for $q = 2$ and (41) for a general $q > 1$ in Sect. 4.2.2).

4.2.1 Regime **I**

The solution of (24) is a density with finite support $[L_1, L_2]$ where $L_1 \geq 0$. As the density is expected to be smooth, we must have $\rho_c(L_2) = 0$ and $\rho_c(L_1) = 0$ at least for $L_1 > 0$. As the eigenvalues λ_i are nonnegative, another possibility is that $L_1 = 0$ and $\rho_c(L_1) \neq 0$ – this will be regime **II**. The first case, i.e. with $L_1 > 0$ and $\rho_c(L_1) = 0$, defines the regime **I** and is valid for $1 \leq s < s_1(q)$ with s_1 given in (15), as we shall see shortly.

In this subsection, we show that, for $1 \leq s < s_1(q)$ (regime **I**), $\mu_1 < 0$ and $\mu_2 > 0$, hence the effective potential $V(x)$ defined in (23) has a minimum at a nonzero x: at $x = x^* = (\frac{-\mu_1}{q \mu_2})^{\frac{1}{q-1}} > 0$, as shown by Fig. 4(a). The charges concentrate around this nonzero minimum. Thus the density of charges ρ_c is expected to have a finite support over $[L_1, L_2]$ with $L_1 > 0$ and to vanish at the bounds $L_{1,2}$ (see Fig. 3(a)).

A Simple Case: $q = 2$ Let us begin with the case $q = 2$, where we can find an explicit expression for the density ρ_c and the pdf of the purity $\Sigma_2 = \sum_i \lambda_i^2 = \text{Tr}[\rho_A^2]$. As mentioned in the Introduction, results in this subsection, as well as in subsequent sections dealing with the special case $q = 2$, are an extended version of results in [20] and they partially overlap with those of [21].

We find the solution of (24) for $q = 2$ by using Tricomi formula with $F(x) = V'(x)$ (cf (25)). The solution ρ_c has a finite support $[L_1, L_2]$. By imposing $\rho_c(L_1) = 0 = \rho_c(L_2)$

(regime **I**), we get:

$$\rho_c(x) = \frac{2\mu_2}{\pi} \sqrt{x - L_1} \sqrt{L_2 - x}. \tag{29}$$

The optimal charge density is a semi-circle. At this point, there are six unknown parameters: the constant C in Tricomi's formula; the bounds of the density support L_1 and L_2; the Lagrange multipliers μ_0, μ_1 and μ_2. We also have some constraints to enforce. The two constraints $\rho_c(L_1) = 0 = \rho_c(L_2)$, together with the three constraints $\int \rho_c = 1$, $\int x\rho_c = 1$ and $\int x^2\rho_c = s$ fix the value of the five parameters C, L_1, L_2, μ_1 and μ_2. We get μ_0 by inserting the final expression of ρ_c in (23) for a special value of x, say $x = L_2$.

By imposing these constraints, we find $C = \int \rho_c = 1$, $L_{1,2} = 1 \mp 2\sqrt{s - 1}$, $\mu_1 = -\frac{1}{2(s-1)}$, $\mu_2 = \frac{1}{4(s-1)}$ and $\mu_0 = \frac{1}{2} \ln|s - 1| + \frac{1}{4(s-1)} - \frac{1}{2}$. Therefore we have

$$\rho_c(x) = \frac{\sqrt{L_2 - x} \sqrt{x - L_1}}{2\pi (s - 1)}, \tag{30}$$

with $L_{1,2} = 1 \mp 2\sqrt{s - 1}$. This solution is valid for $L_1 > 0$, i.e. for $s < 5/4$. Thus, regime **I** corresponds to $1 \leq s < s_1(2)$ with $s_1(2) = 5/4$.

In this regime, we have $\mu_1 = -\frac{1}{2(s-1)} < 0$, $\mu_2 = \frac{1}{4(s-1)} > 0$, and the effective potential $V(x) = \mu_0 + \mu_1 x + \mu_2 x^2$ has a minimum for $x = x^* = 1 > 0$. The charges concentrate around this minimum: they form a semi-disk centered at $x^* = 1 = (L_1 + L_2)/2$. The radius of the semi-disk $R = 2\sqrt{s - 1}$ increases with s till L_1 reaches its minimal possible value 0 (for $s = 5/4$).

Finally we compute the saddle point energy. Using the saddle point equation ((23)), we get $E_s[\rho_c] = -\frac{1}{2}(\mu_0 + \mu_1 + \mu_2 s) = -\frac{1}{4} \ln(s - 1) + \frac{1}{8}$, which gives the expression of $\Phi_I(s) = E_s[\rho_c] - E[\rho^*] = E_s[\rho_c] - \frac{1}{4}$ (see (28)). The distribution of the purity Σ_2 is thus given by:

$$P(\Sigma_2 = s/N, N) \propto \exp\{-\beta N^2 \Phi_I(s)\}, \tag{31}$$

where the large deviation function Φ_I is explicitly given by:

$$\Phi_I(s) = -\frac{1}{4} \ln(s - 1) - \frac{1}{8}. \tag{32}$$

General Case: $q > 1$ The same qualitative behaviour holds for a general $q > 1$: in the regime **I**, the effective potential $V(x)$ has a minimum at a nonzero $x = x^* > 0$, the charges accumulate around this minimum. The density ρ_c has a finite support $[L_1, L_2]$ with $L_1 > 0$ and $\rho_c(L_1) = 0 = \rho_c(L_2)$. This regime is valid for $1 \leq s \leq s_1(q)$. The value of the critical point is determined from the analysis of regime **II**: we show that regime **II** is valid for $s > s_1(q)$. Unfortunately, we were not able to obtain explicit expressions for ρ_c and Φ_I in regime **I** for general q (the integral in the Tricomi formula for a general q seems hard to compute analytically).

4.2.2 Regime **II**

As s approaches $s_1(q)$ from below, the lower bound L_1 of the density support tends to zero. As the eigenvalues are non-negative, L_1 cannot be negative. Hence, regime **I** does not exist for $s > s_1(q)$. The critical value $s_1(q)$ is the onset of regime **II**, where the density ρ_c has a finite support $]0, L]$ and vanishes only at the upper bound L (see Fig. 3(b)). We will see that regime **II** is valid for $s_1(q) \leq s \leq s_2(q, N)$ where $s_2(q, N)$ is given in (16).

Within regime **II** and for increasing s, μ_1 increases and becomes positive while μ_2 remains positive. The effective potential $V(x) = \mu_0 + \mu_1 x + \mu_2 x^q$ has thus a minimum at a smaller and smaller value $x = x^*$ that sticks to zero when μ_1 becomes positive (see Fig. 4(b)). The charges concentrate close to the origin.

A Simple Case: $q = 2$ We find the solution of (24) for $q = 2$ by using again the Tricomi formula with $F(x) = V'(x)$ (cf. (25)). We are looking for a solution ρ_c with finite support $[0, L]$. After imposing $\rho_c(L) = 0$, we get:

$$\rho_c(x) = \frac{1}{\pi}\sqrt{\frac{L-x}{x}}[A + Bx],\tag{33}$$

with $A = \mu_1 + \mu_2 L$ and $B = 2\mu_2$.

There are five unknown parameters: the arbitrary constant C in Tricomi's formula; the upper bound of the density support L; the Lagrange multipliers μ_0, μ_1 and μ_2. We also have constraints to enforce. The constraint $\rho_c(L) = 0$ together with the three constraints $\int \rho_c = 1$, $\int x\rho_c = 1$ and $\int x^2\rho_c = s$ fix the value of the four parameters C, L, μ_1 and μ_2. We get μ_0 by inserting the final expression of ρ_c in (23) for a special value of x, say $x = L$.

We find $C = \int \rho_c = 1$, $\mu_1 = 8(L-3)/L^2$, $\mu_2 = 4(4-L)/L^3$ and $\mu_0 = \ln(\frac{L}{4}) - \frac{1}{2} - \mu_1\frac{L}{4}$. The upper bound of the support L is solution of the equation $L^2 - 12L + 16s = 0$. Hence $L = 2(3 \pm \sqrt{9 - 4s})$. Physically the density $\rho_c(x)$ must remain positive for $0 < x < L$. It is not difficult to see that this determines L:

$$L = L(s) = 2(3 - \sqrt{9 - 4s})\tag{34}$$

The upper bound L increases with s and matches smoothly regime **I**: $L = 2 = L_2$ at $s = s_1(2) = 5/4$. The solution of regime **II**, exists as long as $s < 9/4$. However, we shall see that there exists another solution for $s > 2$ that is energetically more favorable. This latter solution will yield regime **III**. The solution of regime **II** is thus valid only for $5/4 < s < 2$.

We have seen that $\mu_1 = 8(L-3)/L^2$ and $\mu_2 = 4(4-L)/L^3$. According to the respective sign of μ_1 and μ_2, we distinguish three phases for the effective potential $V(x) = \mu_0 + \mu_1 x + \mu_2 x^2$:

– $2 \leq L < 3$ (i.e. $5/4 \leq s < 27/16$): $\mu_1 < 0$ and $\mu_2 > 0$. The potential $V(x)$ has a minimum at a positive $x = x^* = (-\mu_1)/(2\mu_2) = L(3-L)/(4-L)$ (as in regime **I**). x^* decreases when L (or s) increases and reaches 0 at $L = 3$ (see Fig. 4(a)).
– $3 < L < 4$ (i.e. $27/16 < s < 2$): $\mu_1 > 0$ and $\mu_2 > 0$. The potential is monotonic (increasing) on the real positive axis. It has an absolute minimum at $x = 0$ (see Fig. 4(b)).
– $L > 4$ (i.e. $2 < s \leq 9/4$): $\mu_1 > 0$ but $\mu_2 < 0$. The potential is not anymore bounded from below. It increases around the origin, reaches a maximum at $x = x^* = (\mu_1)/(-2\mu_2) = L(L-3)/(L-4)$ and decreases monotonically for $x > x^*$ to $-\infty$ (see Fig. 4(c)). In this phase, the origin is a local minimum and the solution in (33) is metastable. There is actually a second solution in this phase, where one eigenvalue splits off the sea of the other eigenvalues. This second solution becomes energetically more favorable at $s = s_2 \approx 2 + \frac{2^{4/3}}{N^{1/3}}$. The solution of regime **II** in (33) is thus valid only for $s < s_2$. For $s > s_2$, the second solution dominates: this is regime **III**.

Finally, the distribution of the purity Σ_2 in regime **II** is computed by the saddle point method:

$$P(\Sigma_2 = s/N, N) \propto \exp\{-\beta N^2\Phi_{II}(s)\},\tag{35}$$
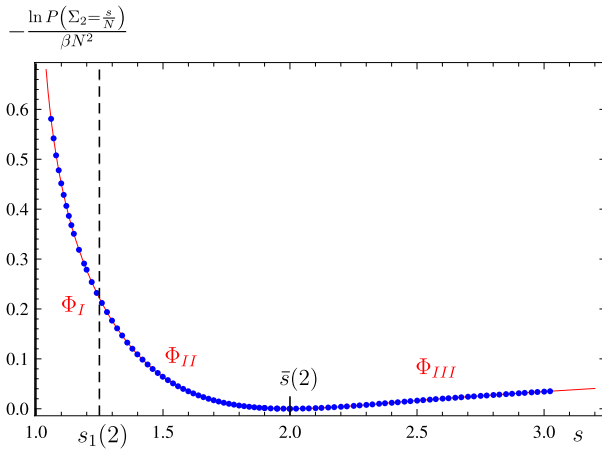
$$-\frac{\ln P\left(\Sigma_2=\frac{s}{N}\right)}{\beta N^2}$$

Fig. 5 (Color online) Distribution of $\Sigma_2 = \sum_i \lambda_i^2$: the figure shows the rate function $\Phi(s) = -\frac{\ln P(\Sigma_2=\frac{s}{N})}{\beta N^2}$ plotted against s for $N = 50$. Analytical predictions (*red solid line*) are compared with the results (*blue points*) of Monte Carlo numerical simulations (method 1, as explained in Sect. 6). Our analytical predictions consist of three regimes. For regimes **I** ($1 \leq s < 5/4$) and **II** ($5/4 < s < 2$), we have plotted the asymptotic expressions of the rate functions in the limit $N \to \infty$ given in (32) and (36). For regime **III**, we have plotted the analytical prediction for large but finite N, using for $\Phi_{III}(s, N) = \Phi(N, s/N)$ (see (51)) the complete expression of E given in (55) and ζ and t (numerical) solutions of (53) and (54). Indeed, for $N = 50$, finite-N corrections to the asymptotic formula in (45) are important in regime **III**: the curve of the dominant behavior in N would not fit well the data and the complete expressions are needed. Note in particular that finite-N effects make that the transition between **II** and **III** is regularized and appears to be smooth

where the large deviation function $\Phi_{II} = E_s[\rho_c] - \frac{1}{4} = -\frac{1}{2}[\mu_1 + \mu_2 s + \mu_0] - \frac{1}{4}$ is explicitely given by:

$$\Phi_{II}(s) = -\frac{1}{2}\ln\left(\frac{L}{4}\right) + \frac{6}{L^2} - \frac{5}{L} + \frac{7}{8}, \tag{36}$$

with $L = 2(3 - \sqrt{9 - 4s})$. For large N, this solution is valid for $s_1(2) < s \leq s_2(2, N)$ with $s_1(2) = 5/4$ and $s_2(2, N) \approx 2 + \frac{2^{4/3}}{N^{1/3}} \to 2$ as $N \to +\infty$ (as we shall see).

At $s = s_1 = 5/4$ (transition between regime **I** and **II**), the rate function $\Phi(s)$ has a weak nonanalyticity. It is continuous, $\Phi(5/4) = -\frac{1}{8} + \frac{\ln 2}{2}$, and even twice differentiable: $\frac{d\Phi}{ds}|_{s=5/4} = -1$ and $\frac{d^2\Phi}{ds^2}|_{s=5/4} = 4$. However, the third derivative is discontinuous: $\frac{d^3\Phi}{ds^3}|_{s=5/4^-} = \frac{d^3\Phi_I}{ds^3}|_{s=5/4} = -32$ but $\frac{d^3\Phi}{ds^3}|_{s=5/4^+} = \frac{d^3\Phi_{II}}{ds^3}|_{s=5/4} = -16$.

For $q = 2$, the authors of [21] studied the Laplace transform of the purity distribution and as a function of their Laplace parameter β, they found a second-order phase transition at $\beta = 2$. When translated into the real space, as a function of the purity itself, this corresponds exactly to the transition we mentioned above at $s = 5/4$ and reported originally in our letter [20]. Interestingly, however, as a function of s, the distribution of purity has a 3-rd order transition at $s = 5/4$ (as shown by the discontinuity in the third derivative of the rate function $\Phi(s)$). On the other hand, in the Laplace space, this corresponds to a second order phase transition [20]. Thus, this is nice example of the fact that the usual ensemble equivalence breaks down due to the presence of long range Coulomb interaction in the system.

The minimum of Φ is reached at $s = 2$ within regime **II**, which gives the mean value of the purity $\langle \Sigma_2 \rangle \approx 2/N$ (as the distribution is highly peaked around its average for large N).

Figure 5 compares our analytical predictions for regimes **I** and **II** in (32) and (36) with numerical data (Monte Carlo simulations): the agreement is very good already for $N = 50$.

General Case: $q > 1$ We find the solution ρ_c with finite support $[0, L]$ of (24) for $q > 1$ by using again the Tricomi formula with $F(x) = V'(x)$ (cf. (25)). After imposing $\rho_c(L) = 0$, we get the expression of the density:

$$\rho_c = \frac{\mu_1}{\pi}\sqrt{\frac{L-x}{x}} + \frac{2\mu_2 q L^{q-1}}{\pi^{3/2}}\frac{\Gamma(q+\frac{1}{2})}{\Gamma(q)}\sqrt{\frac{L-x}{x}}\; {}_2F_1\left(1, 1-q, \frac{3}{2}, 1-\frac{x}{L}\right), \quad (37)$$

where ${}_2F_1$ is a hypergeometric function ${}_2F_1(a, b, c, z) = \sum_{n=0}^{\infty}\frac{(a)_n (b)_n}{(c)_n}\frac{z^n}{n!}$, with $(a)_n = a(a+1)\cdots(a+n-1)$ denoting the raising factorial (Pochhammer symbol).

Exactly as for $q = 2$, the constraints fix the unknown parameters. We obtain the Lagrange multipliers μ_1, μ_2 and μ_0 as functions of L:

$$\mu_1 = \frac{8(1+q)}{(1-q)L^2} - \frac{4q}{L(1-q)} \quad \text{and} \quad \mu_2 = \frac{(1+q)}{(1-q)}\frac{\sqrt{\pi}\,\Gamma(q)}{\Gamma(q+1/2)}\frac{L-4}{L^{q+1}}. \quad (38)$$

and $\mu_0 = \ln(\frac{L}{4}) + \mu_1\frac{L(1-q)}{2q} - \frac{1}{q}$. The upper bound L (which is a function of s) is given by the solution of the equation

$$\left(\frac{1-q}{1+q}\right)L^q + 4L^{q-1} = \frac{2\sqrt{\pi}\,\Gamma(q+1)}{\Gamma(q+1/2)}s. \quad (39)$$

For $q = 2$, we recover the simple expressions of the previous subsection.

The function $f : L \to (\frac{1-q}{1+q})L^q + 4L^{q-1}$ is increasing with L for $0 < L < L_0$ with $L_0 = 4(1+q)/q$, and decreases for $L > L_0$. It is thus maximal at $L = L_0$, which implies that s cannot be larger than $s_0 = s(L = L_0)$ in this regime. Hence, regime **II** is not valid for $s > s_0$, where $s_0 = s_0(q) = s(L = L_0) = \frac{\Gamma(q+1/2)}{2\sqrt{\pi}\Gamma(q+2)}(\frac{4(1+q)}{q})^q$.

Moreover, it can be shown that, for $L < L_0/3$ and for $L > L_0$, the density $\rho_c(x)$ becomes negative for x close to the bounds (close to 0 for $L < L_0/3$, close to L for $L > L_0$). This is not physical. Hence, L must belong to the interval $[L_0/3, L_0]$. Within this range, the function f is monotonic and it increases with L. It can thus be inverted and gives L as a single-valued function of s: $L = L(s)$. This range $[L_0/3, L_0]$ corresponds to $s_1(q) \le s \le s_0(q)$, where $s_1(q) = s(L = L_0/3)$ and $s_0 = s(L = L_0)$.

Therefore regime **II** can exist only for $s_1(q) \le s \le s_0(q)$, where $s_1(q) = \frac{\Gamma(q+3/2)}{\sqrt{\pi}\Gamma(q+2)} \times (\frac{4(1+q)}{3q})^q$ and $s_0(q) = \frac{\Gamma(q+1/2)}{2\sqrt{\pi}\Gamma(q+2)}(\frac{4(1+q)}{q})^q$. For $q = 2$, we recover $s_1(2) = 5/4$ and $s_0(2) = 9/4$. However, as in the $q = 2$ case, this regime is not valid anymore for $s > s_2(q, N)$ given in (16), where a second solution starts to dominate (regime **III**).

Finally, we compute the pdf of Σ_q as a function of $L = L(s)$. We get the pdf by the saddle point method:

$$P(\Sigma_q = N^{1-q}s, N) \propto \exp\{-\beta N^2 \Phi_{II}(s)\}, \quad (40)$$

where the large deviation function $\Phi_{II} = E_s[\rho_c] - \frac{1}{4}$ is explicitly given by:

$$\Phi_{II}(s) = -\frac{1}{2}\ln\left(\frac{L}{4}\right) + \frac{4(1+q)}{qL^2} - \frac{2(1+2q)}{qL} + \frac{3q+1}{4q}. \quad (41)$$

The function $L = L(s)$ is the unique solution of (39) within the range $s_1 \le s \le s_2$.

Exactly as for $q = 2$, the parameter μ_2 (given in (38)) is positive for $L < 4$ ($s < \bar{s}(q)$) and becomes negative for $L > 4$ ($s > \bar{s}(q)$). Hence, for all $q > 1$ the effective potential $V(x) = \mu_0 + \mu_1 x + \mu_2 x^q$ becomes unbounded from below when L exceeds 4. The solution of regime

II is thus metastable in the range $\bar{s}(q) < s < s_0(q)$ ($4 < L < L_0$). Indeed, exactly as for $q = 2$, there exists a second solution for $s > \bar{s}(q)$ that becomes energetically more favorable (lower energy) for $s > s_2(q)$. This is the onset of regime **III**. It occurs at $s = s_2 = \bar{s}$ for very large N, more precisely at $s = s_2(q, N) \approx \bar{s}(q) + [\sqrt{q/2}\,(q-1)\,\bar{s}(q)]^{2q/(2q-1)} / N^{(q-1)/(2q-1)}$ for large but finite N, as we shall see.

As the distribution of Σ_q is highly peaked for large N, its mean value is given by the most probable value: $\langle \Sigma_q \rangle = N^{1-q} \bar{s}(q)$ where $\bar{s}(q)$ minimizes $\Phi(s)$. This minimum $s = \bar{s}(q) = \frac{\Gamma(q+1/2)}{\sqrt{\pi}\Gamma(q+2)}\,4^q$ (or equivalently $L(\bar{s}) = 4$) is reached within regime **II** and $\Phi_{II}(\bar{s}(q)) = 0$. For s close to $\bar{s}(q)$, $\Phi_{II}(s) \approx \frac{(s-\bar{s}(q))^2}{2\sigma_q^2}$ where σ_q^2 is given in (14). We conclude that the distribution of Σ_q has a Gaussian behaviour around its average, as shown in (13), from which we can read the variance (see (14)). For example, for $q = 2$, we have $\sigma_2^2 = 4$ and $\text{Var}\Sigma_2 \approx \frac{4}{\beta N^4}$.

4.3 Regime **III**

As s exceeds $\bar{s}(q)$, μ_2 becomes negative and the effective potential $V(x) = \mu_0 + \mu_1 x + \mu_2 x^q$ is not anymore bounded from below. The solution of regime **II** becomes metastable. The minimum of the potential at the origin still exists, as $V(x)$ increases for small x, but it is a local minimum: $V(x)$ reaches a maximum at $x = x^* > 0$ and then decreases to $-\infty$ (see Fig. 4(c)). Actually, for $s > \bar{s}(q)$, there exists another solution where one charge splits off the sea of the other $(N - 1)$ charges that remain confined close to the origin (in the local minimum of V). The maximal eigenvalue (charge) becomes much larger than the other (see Fig. 3(c)). At some point $s = s_2(q, N)$ very close to $\bar{s}(q)$ for large N, this second solution becomes energetically more favorable than the solution of regime **II**: this is the onset of regime **III**. This phase transition occurs at $s = s_2(q, N)$ given in (42). It is reminiscent of the real-space condensation phenomenon observed in a class of lattice models for mass transport, where a single lattice site carries a thermodynamically large mass [47, 48].

4.3.1 Regime **III**: Summary of Results

We show in this section that there is an abrupt transition from regime **II** to **III** at $s = s_2(q, N)$ where:

$$s_2(q, N) \approx \bar{s}(q) + \frac{[\sqrt{q/2}\,(q-1)\,\bar{s}(q)]^{2q/(2q-1)}}{N^{(q-1)/(2q-1)}} \quad \text{for large } N. \tag{42}$$

Here, $\bar{s}(q)$ the mean value of s given in (12). The maximal eigenvalue t suddenly jumps from a value $t \approx T/N$ very close to the upper edge ζ of the sea of eigenvalues to a value $t \approx [s - \bar{s}(q)]^{1/q}/N^{1-\frac{1}{q}}$ much larger than the other eigenvalues ($t \gg \zeta$) (see Fig. 3(c)). This is clearly shown by the good agreement between our predictions and numerical simulations in Fig. 7 for $N = 500$ and $N = 1000$. The consequence of this phase transition in the Coulomb gas is an abrupt change in the distribution of Σ_q. More precisely, we show that for large N:

$$P(\Sigma_q = N^{1-q} s, N) \approx \exp\left\{-\beta N^{1+\frac{1}{q}}\,\Psi_{III}(s)\right\} \quad \text{for } s > s_2(q, N), \tag{43}$$

where

$$\Psi_{III}(s) = \frac{[s - \bar{s}(q)]^{1/q}}{2}. \tag{44}$$

The expression of the mean value $\bar{s}(q)$ is given in (12). For example, for $q = 2$, this implies:

$$P\left(\Sigma_2 = \frac{s}{N}, N\right) \approx \exp\{-\beta N^{\frac{3}{2}} \Psi_{III}(s)\} \quad \text{with } \Psi_{III}(s) = \frac{\sqrt{s-2}}{2}. \qquad (45)$$

The rate function $\Phi(N, s/N)$ defined by

$$N^2 \Phi(N, s/N) = \begin{cases} N^2 \Phi_{II}(s) & \text{for } s < s_2, \\ N^{1+\frac{1}{q}} \Psi_{III}(s) & \text{for } s > s_2, \end{cases} \qquad (46)$$

is continuous but its derivative is discontinuous at $s = s_2$: for large N we have $\frac{d\Phi}{ds}|_{s_2^+} \approx \frac{d\Phi}{ds}|_{s_2^-}/(2q)$. At the transition point $s = s_2$, there is also a change of concavity of the curve: the rate function in regime **II** is convex ($\frac{d^2\Phi_{II}}{ds^2} > 0$ for $s < s_2$) and has a minimum at $s = \bar{s}$, whereas the rate function in regime **III** is concave ($\frac{d^2\Psi_{III}}{ds^2} < 0$ for $s > s_2$).

Figure 6 shows the transition from regime **II** to regime **III** for $q = 2$ and $N = 1000$: analytical prediction for large N in (45) compare well with Monte Carlo numerical simulations.

4.3.2 New Saddle Point

We want to describe the regime where a single charge (the maximal eigenvalue) detaches from the continuum of the other charges. The assumption that all the eigenvalues are close to each other and can be described by a continuous density of states does not hold anymore. The saddle point must be slightly revised.

We write $\lambda_{max} = t$ and label the remaining $(N-1)$ eigenvalues by a continuous density $\rho(\lambda) = \frac{1}{N-1} \sum_{i \neq max} \delta(\lambda - \lambda_i)$. Physically, as the effective potential has a local minimum at the origin $x = 0$, we expect the optimal charge density ρ_c to have a finite support over $[0, \zeta]$ with $\zeta < t$ and $\rho_c(\zeta) = 0$: while one charge (the maximal eigenvalue t) splits off the sea, the other charges (the sea) remain confined close to the origin (in the local minimum of V, see Fig. 4(c)).

In this regime, we do not rescale the density (and the energy) by assuming that $\lambda \sim 1/N$. We want indeed to compute the pdf of $\Sigma_q = S$ for all $\bar{S}(q) \leq S \leq 1$, where $\bar{S}(q) = N^{1-q} \bar{s}(q)$. The effective energy is now a function of both t and ρ:

$$E_S[\rho, t] = -\frac{(N-1)^2}{2} \int_0^\zeta \int_0^\zeta d\lambda d\lambda' \, \rho(\lambda)\rho(\lambda') \ln|\lambda - \lambda'|$$

$$- (N-1) \int_0^\zeta d\lambda \, \rho(\lambda) \ln|t - \lambda| + \mu_0\left(\int_0^\zeta d\lambda \, \rho(\lambda) - 1\right)$$

$$+ \mu_1\left((N-1) \int_0^\zeta d\lambda \, \lambda \, \rho(\lambda) + t - 1\right)$$

$$+ \mu_2\left((N-1) \int_0^\zeta d\lambda \, \lambda^q \, \rho(\lambda) + t^q - S\right). \qquad (47)$$

The dominating configuration is described by the optimal charge density ρ_c and the optimal value t_c of $t = \lambda_{max}$ such that:

$$\frac{\delta E_S}{\delta \rho}\bigg|_{\rho=\rho_c, t=t_c} = 0 \quad \text{and} \quad \frac{\partial E_S}{\partial t}\bigg|_{\rho=\rho_c, t=t_c} = 0. \qquad (48)$$

Taking into account the normalization, we have indeed for large N: $P(\Sigma_q = S, N) \approx$ $\frac{\int \mathcal{D}\rho \int dt \, e^{-\beta E_S[\rho,t]}}{\int \mathcal{D}\rho \int dt \, e^{-\beta E[\rho,t]}} \approx \exp\{-\beta(E_S[\rho_c, t_c] - E[\rho^*, t^*])\}$, where $E_S[\rho, t]$ is given in (47) and $E[\rho, t]$ has the same expression as $E_S[\rho, t]$ but without the last term (the constraint $\sum_i \lambda_i^q = S$). The pair (ρ^*, t^*) (resp. (ρ_c, t_c)) minimizes $E[\rho, t]$ (resp. $E_S[\rho, t]$). In fact, the normalization is given by the saddle point energy evaluated at $S = \bar{S}$ (the mean value of S): $E[\rho^*, t^*] = E_S[\rho_c, t_c]|_{S=\bar{S}}$ (with $\bar{S} = 2/N$ for $q = 2$). We shall see that for large N, we have:

$$E[\rho^*, t^*] = E_S[\rho_c, t_c]\big|_{S=\bar{S}} \approx N^2 \left(\frac{\ln N}{2} + \frac{1}{4} \right). \tag{49}$$

Formally, by analogy with regimes **I** and **II**, we can write:

$$P(\Sigma_q = S, N) \approx \exp\{-\beta N^2 \Phi(N, S)\}, \tag{50}$$

where we define the rate function Φ as

$$\Phi(N, S) = (E_S[\rho_c, t_c] - E[\rho^*, t^*])/N^2. \tag{51}$$

However, we shall see that the scaling of Φ with N is different in regime **III** with respect to the regimes **I** and **II**. In regimes **I** and **II**, Φ was independent of N for large N: $\Phi(N, s/N) \to \Phi_I(s)$ (resp. $\Phi_{II}(s)$). In regime **III**, we shall see that: $\Phi(N, s/N) \approx \Psi_{III}(s)/N^{1-\frac{1}{q}}$ for large N.

For simplicity, we write t instead of t_c in the following.

4.3.3 Case $q = 2$

Following the same steps as for regime **II**, we find that the optimal charge density is explicitly given for $q = 2$ by:

$$\rho_c(\lambda) = \frac{1}{\pi (N-1)} \sqrt{\frac{\zeta - \lambda}{\lambda}} \left[A + B\lambda + \frac{C}{t - \lambda} \right], \tag{52}$$

with $A = \frac{4}{\zeta^2}[N\zeta - 2 + 2\sqrt{t(t-\zeta)}]$, $B = \frac{8}{\zeta^3}[4 - N\zeta + \sqrt{\frac{t}{t-\zeta}}(3\zeta - 4t)]$ and $C = \sqrt{\frac{t}{t-\zeta}}$, where ζ and $t = t_c$ satisfy:

(a) $\quad 16S + N\zeta^2 - 12\zeta - \sqrt{\frac{t}{t-\zeta}}(16t^2 - 20t\zeta + 5\zeta^2) = 0, \tag{53}$

(b) $\quad (8t^2 - 8t\zeta + \zeta^2)^2 = 8(t - \zeta)\sqrt{t(t-\zeta)}(8t - 2\zeta - 2Nt\zeta + N\zeta^2). \tag{54}$

These equations can be solved numerically for every $\Sigma_2 = S$. We can also find the solutions analytically for very large N.

For $S = \frac{s}{N}$ with $2 < s < 9/4$, there exist two solutions for the pair (ζ, t). The first solution is of the form $t \approx \zeta$ with $\zeta \approx O(1/N)$. This is exactly (to leading order in N) the solution of regime **II** (see below, "first solution"). There is also a second solution, where $t \gg \zeta$: the maximal eigenvalue becomes much larger than the other eigenvalues. More precisely, $\zeta \approx O(1/N)$ whereas $t \approx O(1/\sqrt{N})$ for $S \approx O(1/N)$ (see below, "second solution"). We shall see that the first solution (regime **II**) is valid up to a value $s = s_2 \approx 2 + \frac{2^{4/3}}{N^{1/3}}$ for large N, whereas the solution with $t \gg \zeta$ starts to dominate for $s > s_2$ (its energy becomes lower): this is regime **III**.

For $S > \frac{9}{4N}$ ($s > \frac{9}{4}$), there remains only one solution (the second one), where $\zeta = L/N$ and $t \gg \zeta$.

Note that in both cases, for large N (and for $\frac{2}{N} \leq S < 1$), the upper bound ζ remains of the order $\sim O(1/N)$. We shall thus write $\zeta = \frac{L}{N}$ with $L \sim O(1)$. On the other hand, the maximal eigenvalue t scales from $O(1/N)$ (as $S \to 2/N$) to $O(1)$ (as $S \to 1^-$).

Finally, we compute the saddle point energy as a function of $\zeta = L/N$ and t. As finite-size effects (large but finite N) are important in this regime, we keep all terms up to order $O(N)$ in the saddle point energy, which gives:

$$E_S[\rho_c, t] = E(\zeta, t) = -\frac{(N-1)^2}{2} \ln\left[\frac{\zeta}{4}\right] - 2N \ln\left[\frac{\sqrt{t} + \sqrt{t - \zeta}}{2}\right] + \frac{1}{2} \ln[t(t - \zeta)]$$

$$+ \frac{9N^2}{8} + \frac{6(1 + t^2)}{\zeta^2} - \frac{5(N + t)}{\zeta} + \frac{t}{8(t - \zeta)}$$

$$+ \sqrt{\frac{t}{t - \zeta}} \left[-\frac{19N}{4} - \frac{12t}{\zeta^2} + \frac{11}{\zeta} + \frac{5Nt}{\zeta}\right], \tag{55}$$

where $\zeta = \zeta(s)$ and $t = t_c = t(s)$ are given by (53) and (54).

The rate function is thus given by $\Phi(N, S) = (E_S[\rho_c, t] - E[\rho^*, t^*])/N^2 = (E[\zeta, t] - E[\rho^*, t^*])/N^2$ with $E[\zeta, t]$ given in (55).

Scaling $S = s/N$ with $s \sim O(1)$: First Solution $t \approx \zeta$ with $\zeta \sim O(1/N)$ (Regime II) For $S = \frac{s}{N}$ with $s \sim O(1)$ for large N, the solution of regime **II** still exists as long as $s < 9/4$ (where $9/4 = s_0(2)$). We recover this solution from the (53) and (54) with the scaling $t = \frac{T}{N}$ and $\zeta = \frac{L}{N}$ with $T \approx L \sim O(1)$, i.e. the maximal eigenvalue t remains very close to the other eigenvalues ($t \approx \zeta$ for large N).

In this limit, equations (53) and (54) indeed give:

$$\text{(a)} \quad 16s + L^2 - 12L \approx 0, \tag{56}$$

$$\text{(b)} \quad (T - L)^{3/2} \approx \frac{L^{5/2}}{8(6 - L)} \frac{1}{N}. \tag{57}$$

Equation (a) is the same as (39) of regime **II**. To leading order in N (order N^2), (55) reduces to:

$$E_S[\rho_c, t] = E(L, t) = -\frac{N^2}{2} \ln\left(\frac{L}{4}\right) + 6\frac{N^2}{L^2} - 5\frac{N^2}{L} + N^2\left(\frac{\ln N}{2} + \frac{9}{8}\right). \tag{58}$$

Therefore, using (49), we get $\Phi(N, s/N) = (E_S[\rho_c, t] - E_S[\rho_c, t]|_{s=2})/N^2 = \Phi(s)$ with $\Phi(s) = -\frac{1}{2} \ln(\frac{L}{4}) + \frac{6}{L^2} - \frac{5}{L} + \frac{7}{8} = \Phi_{II}(s)$. We recover the expression in (36) of regime **II**.

However, for $S = s/N > 2/N$ there exists a second solution that becomes energetically more favorable at some point $s_2 \approx 2 + \frac{2^{4/3}}{N^{1/3}}$. Therefore regime **II** is only valid for $5/4 < s < s_2$.

Scaling $S = s/N$ with $s \sim O(1)$: Second Solution $t \gg \zeta$ (Regime III) For $S = s/N$ with $s > 2$, there exists a second solution where one eigenvalue ($\lambda_{\max} = t$) becomes much larger than the others: $t \gg \zeta$. In this limit, (53) and (54) give for large N:

$$t \approx \frac{\sqrt{s - 2}}{\sqrt{N}} \quad \text{and} \quad \zeta \approx \frac{4}{N}\left[1 + \frac{3 - s}{\sqrt{s - 2}} \frac{1}{\sqrt{N}}\right]. \tag{59}$$
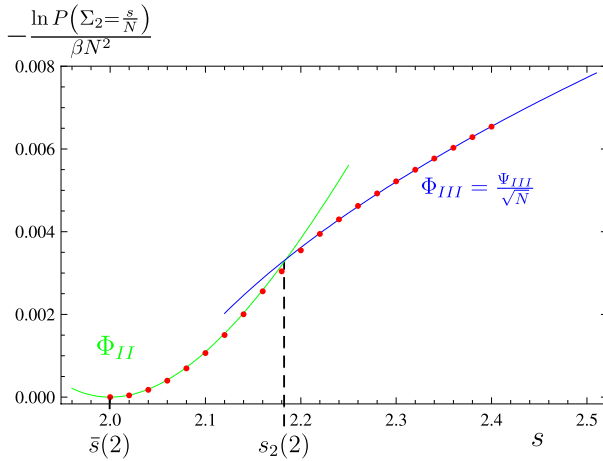
Fig. 6 (Color online) Distribution of Σ_2: rate function $\Phi = -\ln P[\Sigma_2 = s/N]/(\beta N^2)$ plotted against s for $N = 1000$. Analytical results (*solid line*) are compared with data (*red points*) of numerical simulations (Monte Carlo, method 2, see Sect. 6). Analytical results here are the rate functions expected in the limit of very large N: $\Phi_{II}(s)$ in regime **II** (*green solid line*, see (36)) and $\Phi(N, s/N) \approx \Psi_{III}(s)/\sqrt{N}$ in regime **III** (*blue solid line*, see (45)). The transition between regimes **II** and **III** is abrupt, we can see the discontinuity of the derivative of the rate function. It occurs at $s_2(q = 2, N) \approx 2 + \frac{2^{4/3}}{N^{1/3}} - \frac{2^{5/3} \ln N}{3 N^{2/3}} \approx 2.18$ for $N = 1000$

For $S \to 1$, which implies $s \to \infty$ as $N \to \infty$, we find $t \approx \sqrt{\frac{s}{N}} = \sqrt{S}$ and $\zeta \approx \frac{4}{N}(1 - \sqrt{\frac{s}{N}}) \approx \frac{4}{N}(1 - t)$ as also recovered in (64).

We can expand the saddle point energy in (55) replacing t and ζ by the expressions given in (59) for large N. We obtain:

$$E_S[\rho_c, t] \approx \frac{\sqrt{s-2}}{2} N^{3/2} + N^2 \left(\frac{\ln N}{2} + \frac{1}{4} \right) - \frac{N}{2} \ln N + O(N) \quad \text{for large } N . \quad (60)$$

Finally, we get $N^2 \Phi(N, s/N) = E_{s/N}[\rho_c, t] - N^2(\frac{\ln N}{2} + \frac{1}{4}) \approx \frac{\sqrt{s-2}}{2} N^{3/2} - \frac{N}{2} \ln N + O(N)$ for large N (see (49)) and the pdf of Σ_2 is thus given for large N by:

$$P\left(\Sigma_2 = \frac{s}{N}, N \right) \approx e^{-\beta N^{3/2} \Psi_{III}(s)} , \quad (61)$$

where $N^{3/2} \Psi_{III}(s) = N^2 \Phi(N, s/N)$, that is

$$\Psi_{III}(s) = \frac{\sqrt{s-2}}{2} - \frac{\ln N}{2\sqrt{N}} + O\left(\frac{1}{\sqrt{N}} \right) \approx \frac{\sqrt{s-2}}{2} \quad \text{for large } N . \quad (62)$$

The rate function has a very different behaviour for large N in regime **II** and **III**. In regime **I** and **II**, we have $P(\Sigma_2 = \frac{s}{N}, N) \approx e^{-\beta N^2 \Phi(s)}$, whereas in regime **III** we have $P(\Sigma_2 = \frac{s}{N}, N) \approx e^{-\beta N^{3/2} \Psi_{III}(s)}$. For large but finite N and for $s > 2$ but very close to $\bar{s} = 2$, we have $N^{3/2} \Psi_{III}(s) > N^2 \Phi_{II}(s)$. Therefore the solution of regime **II** dominates close to $s = 2$. However, the solution of regime **III** becomes energetically more favorable at some point s_2 defined by $N^{3/2} \Psi_{III}(s_2) = N^2 \Phi_{II}(s_2)$, that is

$$s_2 \approx 2 + \frac{2^{4/3}}{N^{1/3}} - \frac{2^{5/3} \ln N}{3 N^{2/3}} \quad \text{for large } N . \quad (63)$$

At $s = s_2$, there is an abrupt transition from regime **II** to **III**. The maximal eigenvalue t jumps from a value $t \approx \frac{T}{N}$ with $T \sim O(1)$ and t very close to ζ to a value $t \approx \frac{\sqrt{s-2}}{\sqrt{N}}$ much larger than the other eigenvalues ($t \gg \zeta$). The rate function is continuous but its derivative is discontinuous: $N^2 \frac{d\Phi_{II}}{ds}|_{s=s_2^-} \approx \frac{N^{5/3}}{2^{2/3}}$, whilst $N^{3/2} \frac{d\Psi_{III}}{ds}|_{s=s_2^+} \approx \frac{N^{5/3}}{4\,2^{2/3}}$ for large N. At the transition point $s = s_2$, there is also a change of concavity of the curve: the rate function in regime **II** is convex ($\frac{d^2\Phi_{II}}{ds^2} > 0$ for all $s < 9/4$) and has a minimum at $s = \bar{s} = 2$, whereas the rate function in regime **III** is concave ($\frac{d^2\Psi_{III}}{ds^2} < 0$ for all $s > 2$).

Scaling $\Sigma_2 = S \approx O(1)$ and Limit $S \to 1$ (Unentangled State) In the far-right tail of the distribution $\Sigma_2 = S \approx O(1)$ ($S \gg s/N$, $S \le 1$) and the maximal eigenvalue $t \approx O(1)$ whereas ζ (and all the other eigenvalues) remain of order $O(1/N)$. In this limit, equations (53) and (54) become:

$$S \approx t^2 \quad \text{and} \quad L \approx 4(1-t) \quad \text{as } t \approx O(1). \tag{64}$$

The saddle point energy in (55) reduces to: $E_S[\rho_c, t] \approx -\frac{N^2}{2} \ln(1-t) + N^2(\frac{\ln N}{2} + \frac{1}{4}) - N \ln N + O(N)$ as $S \approx O(1)$ with $t = \sqrt{S}$. Using (49), we get an explicit expression for the rate function $\Phi(N, S) = (E_S[\rho_c, t_c] - E[\rho^*, t^*])/N^2$ for large N:

$$\Phi(N, S) \approx \frac{(E_S[\rho_c, t] - N^2(\frac{\ln N}{2} + \frac{1}{4}))}{N^2} \approx -\frac{1}{2} \ln(1 - \sqrt{S}) \equiv \Phi_{III}(S). \tag{65}$$

We conclude that

$$P(\Sigma_2 = S, N) \approx e^{-\beta N^2 \Phi_{III}(S)} \approx (1 - \sqrt{S})^{\frac{\beta N^2}{2}} \quad \text{for large } N, \text{ fixed } S. \tag{66}$$

The difference of scaling with respect to regimes **I** and **II** comes from the scaling of Σ_2: in regimes **I** (resp. **II**), we had $\Phi(N, s/N) \to \Phi_I(s)$ (resp. $\Phi_{II}(s)$) for large N, whereas here we have: $\Phi(N, S) \to \Phi_{III}(S)$ for large N and fixed $S \approx O(1)$. As $S = s/N$ with fixed s and large N, which corresponds to the limit $S \to 0$ in this scaling, we find $N^2 \Phi_{III}(S) \approx N^{3/2} \sqrt{s}/2$ which is also the limit $s \to \infty$ of $N^{3/2} \Psi_{III}(s)$. The right tail (where $S \approx O(1/N)$) and the far-right tail (where $S \approx O(1)$) of the distribution match smoothly.

As $\Sigma_2 = S$ tends to its maximal value 1, the maximal eigenvalue $t \to 1$ and $L \to 0$. At $S = 1$, only one eigenvalue, the maximal one $\lambda_{max} = t$, is nonzero (and equal to one). This corresponds to an unentangled state (situation (i)). The probability of an unentangled state (i.e. $\Sigma_2 \to 1$) is thus vanishingly small for large N.

4.3.4 General $q > 1$

Using again Tricomi's theorem and imposing the constraints $\int \rho_c = 1$ and $\rho_c(\zeta)$, we find that the optimal charge density for the $N - 1$ smallest eigenvalues is given by:

$$\rho_c(\lambda) = \frac{1}{\pi(N-1)} \sqrt{\frac{\zeta - \lambda}{\lambda}} \left[A + B \, {}_2F_1\left(1, 1-q, \frac{3}{2}, 1 - \frac{\lambda}{\zeta}\right) + \frac{C}{t - \lambda} \right], \tag{67}$$

where $A = \mu_1$, $B = \mu_2 2q\zeta^{q-1} \frac{\Gamma(q+1/2)}{\sqrt{\pi}\Gamma(q)}$ and $C = \sqrt{\frac{t}{t-\zeta}}$ and ${}_2F_1$ is a hypergeometric function ${}_2F_1(a, b, c, z) = \sum_{n=0}^{\infty} \frac{(a)_n (b)_n}{(c)_n} \frac{z^n}{n!}$, with $(a)_n = a(a+1)\cdots(a+n-1)$ denoting the raising
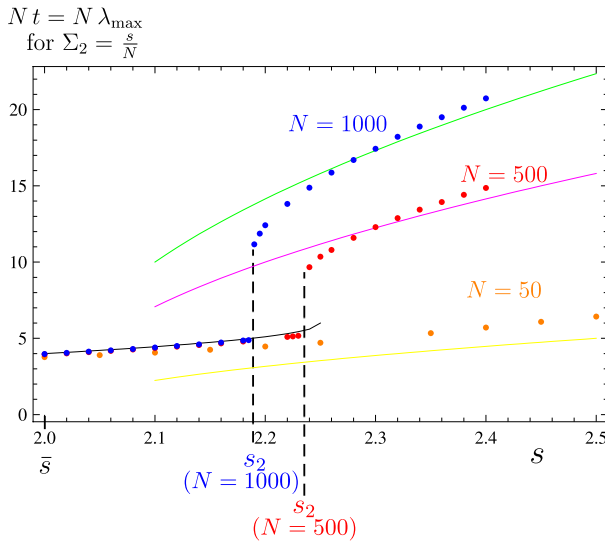
Fig. 7 (Color online) Maximal eigenvalue $\lambda_{\max} = t$ corresponding to a fixed value of the purity $\Sigma_2 = s/N$ plotted against s for different values of N. Analytical predictions (*solid lines*) are compared with numerical simulations (*points*: Monte Carlo data, method 2 with density). The theory predicts for large N a sudden jump of t from a value $t \approx \zeta = L(s)/N$ with $L(s) = 2(3 - \sqrt{9 - 4s})$ (within regime **II**, $s < s_2$) to a much larger value $t \approx \frac{\sqrt{s-2}}{\sqrt{N}}$ (regime **III**, $s > s_2$). We clearly see this jump in numerical simulations for $N = 500$ at $s_2 \approx 2.23$ and $N = 1000$ at $s_2 \approx 2.18$. For $N = 50$, finite-size corrections to the large N asymptotics are considerable enough to smear the jump in t. Because of the choice of scaling on the plot, tN as a function of s, the plots of the maximal eigenvalue in regime **II** are expected to be the same for different N (for large N), whereas the plots for regime **III** differ by a factor $\sqrt{N}$

factorial (Pochhammer symbol). The Lagrange multipliers μ_1 and μ_2 are given by:

$$\mu_1 = \frac{4}{(q-1)\zeta^2}\left[qN\zeta - 2(q+1) + \sqrt{\frac{t}{t-\zeta}}\{(2q+2)t - (2q+1)\zeta\}\right],$$

$$\mu_2 = \frac{\sqrt{\pi}\,\Gamma(q+2)}{\zeta^{q+1}\Gamma(q+1/2)q(q-1)}\left[4 - N\zeta + \sqrt{\frac{t}{t-\zeta}}\{3\zeta - 4t\}\right], \tag{68}$$

where ζ and t are solutions of the following system of equations:

$$\text{(a)}\quad S - t^q = \frac{\zeta^{q-1}\Gamma(q+1/2)}{\sqrt{\pi}\,\Gamma(q+1)}\left\{2 - \frac{N\zeta}{2}\left(\frac{q-1}{q+1}\right) + \sqrt{\frac{t}{t-\zeta}}\left[\zeta\left(\frac{3q+1}{2q+2}\right)\right.\right.$$

$$\left.\left. - 2t\right]\right\} + \sqrt{\frac{t}{t-\zeta}}\frac{\zeta^{q+1}\Gamma(q+1/2)}{2t\sqrt{\pi}\,\Gamma(q+2)}\,{}_2F_1\left(1, q+\frac{1}{2}, 2+q, \frac{\zeta}{2}\right), \tag{69}$$

$$\text{(b)}\quad \mu_1\sqrt{\frac{t-\zeta}{t}} + q\mu_2 t^{q-1} = \frac{\zeta}{2t(t-\zeta)} + \mu_2\frac{\zeta^q\Gamma(q+\frac{1}{2})}{t\sqrt{\pi}\,\Gamma(q)}\,{}_2F_1\left(1, q, q+1, \frac{\zeta}{t}\right), \tag{70}$$

with $\mu_1 = \mu_1(\zeta, t)$ and $\mu_2 = \mu_2(\zeta, t)$ given in (68).

These equations can be solved analytically for large N and the solutions are qualitatively the same as for $q = 2$.

For $S = N^{1-q} s$ with $\bar{s}(q) < s < s_0(q)$ (where $s_0(q) = \frac{\Gamma(q+1/2)}{2\sqrt{\pi}\Gamma(q+2)}(\frac{4(1+q)}{q})^q$, see regime **II**), there exist two different solutions for the pair (ζ, t). The first solution is of the form $t \approx \zeta$ with $\zeta \approx O(1/N)$. This is exactly (to leading order in N) the solution of regime **II** (see below, "first solution"). There is also a second solution with $t \gg \zeta$, more precisely $\zeta = L/N$ with $L \sim O(1)$ and $t \approx O(1/N^{1-1/q})$ for $S \approx N^{1-q} s$, and $\zeta \approx O(1/N)$ (see below, "second solution"). For s close to $\bar{s}(q)$, the first solution dominates (regime **II**), but at some point $s = s_2(q, N) > \bar{s}(q)$ given in (74), the second solution, with $t \gg \zeta$, starts to dominate (its energy becomes lower): this is regime **III**.

For $S > N^{1-q} s_0(q)$, i.e. $s > s_0$, only the second solution remains: the upper bound of the density support scales as $\zeta = L/N$ with $L \sim O(1)$ while the maximal eigenvalue is much larger than all other eigenvalues: $t \gg \zeta$.

In both cases (as for $q = 2$), for large N the upper bound ζ remains of order $\sim O(1/N)$ ($\zeta \sim \lambda_{\text{typ}}$). We shall thus write $\zeta = \frac{L}{N}$ with $L \sim O(1)$. On the other hand (as for $q = 2$), the maximal eigenvalue t scales from $O(1/N)$ (as $S \to N^{1-q}\bar{s}(q)$) to $O(1)$ (as $S \to 1^-$).

*Scaling $S = N^{1-q} s$ with $s \sim O(1)$: First Solution $t \approx \zeta$ with $\zeta \sim O(1/N)$ (Regime **II**)*
For $S = N^{1-q} s$ with $s \sim O(1)$ for large N, the solution of regime **II** still exists as long as $s < s_0(q)$. We recover this solution from the (69) and (70) with the scaling $t = \frac{T}{N}$ and $\zeta = \frac{L}{N}$ with $T \approx L \sim O(1)$, where the maximal eigenvalue t remains very close to the other eigenvalues ($t \approx \zeta$ for large N), it does not play a special role. Using (49), we finally get $\Phi(N, s/N) = (E_S[\rho_c, t] - E_S[\rho_c, t]|_{s=2})/N^2 = \Phi_{II}(s)$, the same expression as in (41) of regime **II**.

However, for $s > \bar{s}(q)$ there exists a second solution that becomes energetically more favorable at some point $s_2(q, N)$. Therefore regime **II** is only valid for $s_1 < s < s_2$.

*Scaling $S = N^{1-q} s$ with $s \sim O(1)$: Second Solution $t \gg \zeta$ (Regime **III**)*   For $S = N^{1-q} s$ with $s > \bar{s}(q)$, there exists a second solution where one eigenvalue ($\lambda_{\max} = t$) becomes much larger than the other eigenvalues: $t \gg \zeta$. In this limit, (69) and (70) give for large N:

$$t \approx \frac{[s - \bar{s}(q)]^{1/q}}{N^{1-1/q}} \quad \text{and} \quad \zeta \approx \frac{4}{N}\left[1 - \left\{\frac{s - \bar{s}(q)(1+q)/2}{[s - \bar{s}(q)]^{1-1/q}}\right\}\frac{1}{N^{1-1/q}}\right]. \tag{71}$$

For $S \to 1$, which implies $s \to \infty$ as $N \to \infty$, we find $t \approx s^{1/q} N^{1/q-1} = S^{1/q}$ and $\zeta \approx \frac{4}{N}(1 - t)$.

We can compute the saddle point energy in this limit replacing t and ζ by the expressions given in (71) for large N. Finally, we get $N^2 \Phi(N, s/N) = E_S[\rho_c, t] - N^2(\frac{\ln N}{2} + \frac{1}{4}) \approx N^{1+\frac{1}{q}}\frac{[s-\bar{s}(q)]^{1/q}}{2}$ for large N (see (49)) and the pdf of Σ_q is thus given for large N by:

$$P(\Sigma_q = N^{1-q} s, N) \approx \exp\left\{-\beta N^{1+\frac{1}{q}} \Psi_{III}(s)\right\}, \tag{72}$$

where

$$\Psi_{III}(s) = \frac{[s - \bar{s}(q)]^{1/q}}{2} \quad \text{for large } N. \tag{73}$$

The solution of regime **III** becomes energetically more favorable, that is $N^{1+\frac{1}{q}}\Psi_{III}(s) < N^2 \Phi_{II}(s)$, at some point $s_2(q, N)$ defined by $N^{1+\frac{1}{q}}\Psi_{III}(s_2) = N^2\Phi_{II}(s_2)$. Therefore

$$s_2(q, N) \approx \bar{s}(q) + \frac{[\sqrt{q/2}\,(q-1)\,\bar{s}(q)]^{2q/(2q-1)}}{N^{(q-1)/(2q-1)}} \quad \text{for large } N. \tag{74}$$

At $s = s_2$, there is an abrupt transition from regime **II** to **III**. The maximal eigenvalue t jumps from a value $t \approx \frac{T}{N}$ with $T \sim O(1)$ and t very close to ζ to a value $t \approx \frac{[s - \bar{s}(q)]^{1/q}}{N^{1 - 1/q}}$ much larger than the other eigenvalues ($t \gg \zeta$). The rate function $\Phi(N, s/N)$ given by

$$N^2 \Phi(N, s/N) = \begin{cases} N^2 \Phi_{II}(s) & \text{for } s < s_2, \\ N^{1 + \frac{1}{q}} \Psi_{III}(s) & \text{for } s > s_2, \end{cases} \tag{75}$$

is continuous but its derivative is discontinuous. For large N, we have indeed $N^2 \frac{d\Phi}{ds}\big|_{s_2^-} \approx N^{\frac{3q-1}{2q-1}} \{(q-1)\sqrt{q/2}\, \bar{s}(q)\}^{\frac{2-2q}{2q-1}}$, whilst $\frac{d\Phi}{ds}\big|_{s_2^+} \approx \frac{d\Phi}{ds}\big|_{s_2^-} / (2q)$. At the transition point $s = s_2$, there is also a change of concavity of the curve: the rate function in regime **II** is convex ($\frac{d^2 \Phi_{II}}{ds^2} > 0$) and has a minimum at $s = \bar{s}$, whereas the rate function in regime **III** is concave ($\frac{d^2 \Psi_{III}}{ds^2} < 0$).

5 Distribution of the Renyi Entropy S_q

In Sect. 4, we have computed the full distribution of $\Sigma_q = \sum_{i=1}^N \lambda_i^q$ for large N. A simple change of variable gives the distribution of the Renyi entropy $S_q = \frac{1}{1-q} \ln[\sum_i \lambda_i^q] = \frac{1}{1-q} \ln[\Sigma_q]$. The scaling $\Sigma_q = N^{1-q} s$ for large N implies $S_q = \ln N - \frac{\ln s}{q-1}$. This means that typical values of S_q will be of order $S_q \approx \ln N - z$ with $z \approx O(1)$ for large N. The parameter $z = \frac{\ln s}{q-1}$ is nonnegative and its minimum $z = 0$ corresponds to $S_q = \ln N$, which corresponds to the maximally entangled state.

The distribution of the entropy is thus given for large N by:

$$P(S_q = \ln N - z) \approx \begin{cases} \exp\{-\beta N^2 \phi_I(z)\} & \text{for } 0 < z \leq z_1(q), \\ \exp\{-\beta N^2 \phi_{II}(z)\} & \text{for } z_1(q) < z \leq z_2(q), \\ \exp\{-\beta N^{1+\frac{1}{q}} \psi_{III}(z)\} & \text{for } z > z_2(q). \end{cases} \tag{76}$$

The three regimes are the same as for Σ_q. The rate functions ϕ_I, ϕ_{II} and ψ_{III} are simply obtained from the rate functions Φ_I, Φ_{II} and Ψ_{III} for the distribution of Σ_q (see (11)) by the change of variable $s = \exp[(q-1)z]$, e.g. $\phi_I(z) = \Phi_I(e^{(q-1)z})$. Explicit expressions of the functions Φ_I and Φ_{II} are given in (32) and (36) for $q = 2$, and in (41) for a general $q > 1$; an explicit expression of Ψ_{III} is given in (44) for a general $q > 1$ (and in (45) for $q = 2$).

The critical points are given by

$$z_1(q) = \frac{\ln s_1(q)}{q - 1} \quad \text{and} \quad z_2(q, N) = \frac{\ln s_2(q, N)}{q - 1}, \tag{77}$$

where s_1 and s_2 are the critical points for Σ_q (see (15) and (16)).

The distribution of the entropy S_q has the same qualitative behaviour as that of Σ_q: it is a highly peaked distribution with Gaussian behaviour around the mean value and non-Gaussian tails. Again, the average value of S_q coincides with the most probable value for large N, $\langle S_q \rangle \approx \ln N - \bar{z}(q)$ where $\bar{z}(q)$ is the minimum of ϕ_{II}:

$$\langle S_q \rangle \approx \ln N - \bar{z}(q) \quad \text{with} \quad \bar{z}(q) = \frac{\ln \bar{s}(q)}{q - 1} = \frac{1}{q - 1} \ln\left[\frac{\Gamma(q + 1/2)}{\Gamma(q + 2)} \frac{4^q}{\sqrt{\pi}}\right]. \tag{78}$$

The rate function $\phi_{II}(z)$ has a quadratic behaviour around $z = \bar{z}(q)$: $\phi_{II}(z) \approx \frac{(z - \bar{z}(q))^2}{q}$. Therefore, the distribution of the entropy S_q has a Gaussian behaviour around its average:

$$P(S_q = \ln N - z) \approx \exp\left\{ -\beta N^2 \frac{(z - \bar{z}(q))^2}{q} \right\} \quad \text{for } z \approx \bar{z}(q), \tag{79}$$

which gives the variance of the distribution:

$$\text{Var } S_q \approx \frac{q}{2\beta N^2} \quad \text{for large } N. \tag{80}$$

5.1 Limit $q \to 1^+$: von Neumann Entropy

As $q \to 1^+$, the Renyi entropy S_q tends to the von Neumann entropy $S_{\text{VN}} = -\sum_i \lambda_i \ln \lambda_i$. The limit $q \to 1$ is singular for the distribution of Σ_q: because of the constraint $\Sigma_1 = \sum_i \lambda_i = 1$, the distribution tends to a Dirac-δ function. The variance tends to zero ($\sigma_q^2 \to 0$) and the mean value $\bar{s}(q)$ as well as the critical point $s_1(q)$ and $s_2(q)$ tend to 1. However, due to the factor $1/(1 - q)$ in the definition of S_q, the limit $q \to 1$ is not at all singular for the entropy S_q. Taking this limit only requires to be careful. For S_{VN} (as for S_q for $q > 1$), there are three regimes in the distribution:

$$P(S_{\text{VN}} = \ln N - z) \approx \begin{cases} \exp\{-\beta N^2 \, \phi_I(z)\} & \text{for } 0 < z \le z_1, \\ \exp\{-\beta N^2 \, \phi_{II}(z)\} & \text{for } z_1 < z \le z_2, \\ \exp\{-\beta \frac{N^2}{\ln N} \, \phi_{III}(z)\} & \text{for } z > z_2, \end{cases} \tag{81}$$

where ϕ_{II} and ϕ_{III} are respectively given in (84) and (88). We could not compute explicitly ϕ_I (as we could not compute Φ_I for the Renyi entropy for a general $q > 1$ except for $q = 2$). For $q \to 1$, we get: $\bar{z}(q) = \frac{\ln \bar{s}(q)}{q-1} \to 1/2$ (where $\bar{z}(q)$ is given in (78)). We thus recover the already known mean value of the von Neumann entropy (see [4]) in the case $c = 1$ ($M \approx N$):

$$\langle S_{\text{VN}} \rangle \approx \ln N - \frac{1}{2} \quad \text{for large } N. \tag{82}$$

The critical points separating the three regimes are given by (limit $q \to 1$ in (77) and (15)):

$$z_1 = \frac{2}{3} - \ln \frac{3}{2} \approx 0.26 \quad \text{and} \quad z_2 \approx \bar{z} = \frac{1}{2}. \tag{83}$$

We easily obtain the expression of the rate function ϕ_{II} in regime **II** by taking the limit $q \to 1$. We get:

$$\phi_{II}(z) = -\frac{1}{2} \ln \left(\frac{L}{4} \right) + \frac{8}{L^2} - \frac{6}{L} + 1, \tag{84}$$

where $L = L(z)$ is the solution of (limit $q \to 1$ in (39))

$$\ln \left(\frac{L}{4} \right) - \frac{L}{8} + 1 = z. \tag{85}$$

For large N, the mean value corresponds to the minimum of ϕ_{II}. The quadratic approximation of ϕ_{II} around this minimum $z \approx \bar{z}$ gives the Gaussian behaviour of the pdf of S_{VN}

around its average and thus the variance in the large N limit:

$$\langle S_{\text{VN}} \rangle \approx \ln N - \bar{z} \quad \text{with } \bar{z} = \frac{1}{2} \quad \text{and} \quad \text{Var } S_{\text{VN}} \approx \frac{1}{2\beta N^2} \, . \tag{86}$$

The limit $q \to 1$ for the regime **III** is a bit more subtle. We would expect the rate function to be of the form $N^2 \psi_{III}(z)$, but $\psi_{III} = \Psi_{III}(e^{(q-1)z})$ (in (44)) vanishes as $q \to 1$. The rate function actually scales as $N^2/\ln N$ (rather than N^2 as one could naïvely expect). This can be shown by a more detailed analysis of the equations (69) and (70) in the limit $q \to 1$. The solution $t \gg \zeta$ is actually given for $q \to 1$ by:

$$t \approx \frac{z - 1/2}{\ln N} \quad \text{and} \quad \zeta \approx \frac{4}{N} \left(1 + \frac{1 - z}{\ln N} \right). \tag{87}$$

The saddle point energy can be computed in this limit. We finally find:

$$-\ln P(S_{\text{VN}} = \ln N - z) \approx \beta \frac{N^2}{\ln N} (z - 1/2) \, ; \qquad \phi_{III}(z) = z - \frac{1}{2} \, . \tag{88}$$

5.2 Limit $q \to \infty$: Maximal Eigenvalue

As $q \to \infty$ the Renyi entropy S_q tends to $-\ln \lambda_{\max}$ where $\lambda_{\max}$ is the maximal eigenvalue. Again, the limit is singular for the distribution of Σ_q but not for S_q. There are the same three regimes in the distribution of $\lambda_{\max}$ for large N as in the distribution of the Renyi entropy.

For large N, the typical scaling is $S_q \approx \ln N - z$, thus $-\ln \lambda_{\max} \approx \ln N - z$ or $\lambda_{\max} \approx \frac{e^z}{N}$. Setting $t = e^z$, we have $\lambda_{\max} = t/N$. In particular, the mean value is given by $\bar{t}/N$ where $\bar{t} = \lim_{q \to \infty} \exp(\bar{z}(q)) = \lim_{q \to \infty} [\bar{s}(q)]^{\frac{1}{q-1}} = 4$, implying

$$\langle \lambda_{\max} \rangle \approx \frac{4}{N} \, . \tag{89}$$

The first critical point is $t_1 = \lim_{q \to \infty} [s_1(q)]^{\frac{1}{q-1}} = 4/3$. The second critical point is $t_2 = \bar{t} = 4$. The three regimes in the distribution of the maximal eigenvalue are the following:

$$P\left(\lambda_{\max} = \frac{t}{N} \right) \approx \begin{cases} e^{-\beta N^2 \chi_I(t)} & \text{for } 1 < t \leq 4/3 \text{ (reg. } \mathbf{I}), \\ e^{-\beta N^2 \chi_{II}(t)} & \text{for } 4/3 < t \leq 4 \text{ (reg. } \mathbf{II}), \\ e^{-\beta N \chi_{III}(t)} & \text{for } t > 4 \text{ (reg. } \mathbf{III}). \end{cases} \tag{90}$$

The rate functions can be explicitly computed. The rate function in regime **I** is given by:

$$\chi_I(t) = -\frac{1}{2} \ln(t - 1) \quad \text{for } 1 < t \leq 4/3 \, . \tag{91}$$

In regime **II**, we find:

$$\chi_{II}(t) = 4 \frac{(1 - t)}{t^2} - \frac{1}{2} \ln\left(\frac{t}{4} \right) + \frac{3}{4} \quad \text{for } 4/3 < t \leq 4 \, . \tag{92}$$

Finally, in regime **III** the maximal eigenvalue detaches from the sea of the other eigenvalues and we get:

$$\chi_{III}(t) = \frac{\sqrt{t(t - 4)}}{2} - 2\ln(\sqrt{t} + \sqrt{t - 4}) + 2\ln 2 \quad \text{for } t > 4 \, . \tag{93}$$

Again, at the first critical point $t_1 = 4/3$, the rate function χ is continuous and twice differentiable, but its third derivative is discontinuous: $\frac{d^3 \chi_I}{dt^3} = -27$ but $\frac{d^3 \chi_{II}}{dt^3} = -999/64$. The average value $\bar{t} = 4$ is the minimum of χ_{II}. At the second critical point $t_2 = 4$, the rate function is continuous but not differentiable.

Exactly as we did for Σ_q, we can also consider the regime where $\lambda_{\max} = T$ ($T \gg t/N$): the far-right tail of the distribution. We find:

$$P(\lambda_{\max} = T) \approx e^{-\beta N^2 \chi_+(T)} \quad \chi_+(T) = -\frac{1}{2} \ln(1 - T) \quad \text{for } 0 < T < 1, \qquad (94)$$

which matches smoothly regime **III**. We have indeed: $N\chi_{III}(t) \approx N\frac{t}{2}$ as $t \to \infty$ and $N^2 \chi_+(t) \approx N^2 \frac{T}{2} \approx N\frac{t}{2}$ as $T \to 0$ with $T = t/N$.

Ideas of Proof Regimes **II** and **III** can be derived by taking carefully the limit $q \to \infty$ (directly in the expression of the rate function for regime **II** but more carefully for regime **III**). The distribution of $\lambda_{\max}$ can also be computed directly (without taking the limit $q \to \infty$). This gives the same results for regimes **II** and **III** and gives also an explicit expression for regime **I** (where the rate function is not explicitly known for a general $q > 1$). We can actually calculate the cumulative distribution Prob($\lambda_{\max} \leq Z$) by the same Coulomb gas method as before. This is indeed easier to compute because the probability that $\lambda_{\max} \leq Z$ is the probability that all the eigenvalues λ_i are smaller than Z. We can thus compute this probability with the Coulomb gas method, with a continuous density $\rho(x) = 1/N \sum_i \delta(x - \lambda_i N)$ and with the constraint that no eigenvalue exceeds Z:

$$P(\lambda_{\max} \leq Z) \propto \int \mathcal{D}\rho \, e^{-\beta N^2 E_Z[\rho]}. \qquad (95)$$

The energy reads

$$E_Z[\rho] = -\frac{1}{2} \int_0^Z \int_0^Z \rho(x)\rho(x') \ln|x - x'| \, dx \, dx' + \mu_0 \left(\int_0^Z \rho(x)dx - 1 \right)$$
$$+ \mu_1 \left(\int_0^Z x\rho(x)dx - 1 \right), \qquad (96)$$

where the Lagrange multipliers μ_0 and μ_1 enforce the two constraints $\int \rho = 1$ (normalization of the density) and $\int x\rho = 1$ (unit sum of the eigenvalues: $\sum_i \lambda_i = 1$). The saddle point method gives:

$$P(\lambda_{\max} \leq Z) \propto e^{-\beta N^2 E_Z[\rho_c]}, \qquad (97)$$

where ρ_c minimizes the effective energy E_Z. This yields regimes **I** and **II**. Exactly as for S_q, in regime **III**, the maximal eigenvalue detaches from the sea of the other charges (eigenvalues), it must be taken into account separately from the continuous density of the other eigenvalues.

In regime **I**, the optimal charge density has a finite support $[L_1, L_2]$ and vanishes at $L_{1,2}$ (exactly as for Σ_q). We get the rate function χ_I in (91).

In regime **II**, the optimal charge density has a finite support $]0, L]$, vanishes at L but diverges at the origin with a square root divergence (exactly as for Σ_q). We get the rate function χ_{II} in (92). This expression can also be obtained by taking the limit $q \to \infty$ of the expression in (41) of Φ_{II}, valid for a general q (for Σ_q).

In regime **III**, the maximal eigenvalue is much larger than the others and we get χ_{III} in (93). The limit $q \to \infty$ in the rate function ψ_{III} for a general q gives: $\psi_{III} \to t/2$. This is actually equal to $\chi_{III}(t)$ only in the limit $t \to \infty$, but not for all $t > 4$. For $q > 1$, regime **III** is characterized by $t \approx T/N^{1-\frac{1}{q}} \gg \zeta$ as $\zeta \approx L/N$, which becomes $t \approx T/N > \zeta$ in the limit $q \to \infty$. The maximal eigenvalue is larger than the other eigenvalues, but not much larger. We cannot anymore assume $t \gg \zeta$ in the computation of the energy. We must compute carefully the energy $E_S[\rho_c, t]$ in this limit. For this computation, we use the complete expression of E_S: for $q = 2$, this expression was given in (55); for a general q, we have a similar but more complicated expression. We use this expression in the limit where t and ζ are both of order one (with $t > \zeta$) and where $q \to \infty$. We finally get $\chi_{III}(t)$ as given in (93).

5.2.1 Typical Fluctuations Around the Average: Tracy-Widom Distribution

We have seen that the average value of the maximal eigenvalue, in the large N limit, is given by $\langle \lambda_{\max} \rangle \approx 4/N$. Of course, $\lambda_{\max}$ fluctuates around this average from sample to sample. The Coulomb gas method presented in this subsection captures fluctuations $\sim O(1/N)$ around this mean, i.e., large fluctuations that are of the same order of magnitude as the mean itself. We have seen that the probability of such large $\sim O(1/N)$ fluctuations is very small, indicating that they are rare atypical fluctuations. The typical fluctuations around the mean occur at a much finer scale around this mean which is not captured by the Coulomb gas method.

To compute the distribution of such typical fluctuations, we start from the joint distribution in (5). The cumulative probability of the maximum can be written as the multiple integral

$$P(\lambda_{\max} \le Z) \propto \int_0^Z \cdots \int_0^Z P(\lambda_1, \lambda_2, \dots, \lambda_N) d\lambda_1 \, d\lambda_2 \cdots d\lambda_N \qquad (98)$$

Next we can replace the delta function $\delta(\sum_{i=1}^N \lambda_i - 1)$ by its integral representation: $\delta(x) = (1/2\pi i) \int dp e^{px}$ where the integral runs over the imaginary axis. This gives, for $M = N$,

$$P(\lambda_{\max} \le Z) \propto \int \frac{dp}{2\pi i} e^p \int_{[0,Z]} \left[\prod_{i=1}^N d\lambda_i \right] e^{-p \sum_{i=1}^N \lambda_i} \prod_{i=1}^N \lambda_i^{\frac{\beta}{2}-1} \prod_{i<j} |\lambda_i - \lambda_j|^\beta. \qquad (99)$$

Rescaling $\lambda_i \to (\beta/2p)\lambda_i$, one can recast the integral as

$$P(\lambda_{\max} \le Z)$$
$$\propto \int_{-i\infty}^{i\infty} \frac{dp}{2\pi i} e^p \, p^{-\beta N^2/2} \int_{[0,2pZ/\beta]} \left[\prod_{i=1}^N d\lambda_i \right] e^{-\frac{\beta}{2} \sum_{i=1}^N \lambda_i} \prod_{i=1}^N \lambda_i^{\frac{\beta}{2}-1} \prod_{i<j} |\lambda_i - \lambda_j|^\beta.$$
$$(100)$$

The integral over λ_i's is just proportional to the cumulative distribution of the maximum of the Wishart matrix, i.e., the $P^{Wishart}(\lambda_{\max} \le 2pZ/\beta)$. This latter quantity, in the large N limit, is known [49, 50] to converge to a limiting distribution known as the Tracy-Widom distribution [51, 52], i.e,

$$P^{Wishart}(\lambda_{\max} \le y) \to F_\beta \left[\frac{(y - 4N)}{2^{4/3} N^{1/3}} \right] \qquad (101)$$

where $F_\beta(x)$ satisfies a nonlinear differential equation [51, 52]. Using this result in (100), we get, in the large N limit,

$$P(\lambda_{\max} \leq Z) \propto \int_{-i\infty}^{i\infty} \frac{dp}{2\pi i} e^{p-\frac{\beta}{2}N^2 \log(p)} F_\beta\left[\frac{\frac{2p}{\beta}Z - 4N}{2^{4/3}N^{1/3}}\right]. \tag{102}$$

The integral over p can now be evaluated via the saddle point method. To leading order for large N, one can show that the saddle point occurs at $p^* = \beta N^2/2$ that just minimise the exponential factor $e^{p-\frac{\beta}{2}N^2 \log(p)}$. Hence, to leading order in large N, we obtain our main result

$$P(\lambda_{\max} \leq Z) \approx F_\beta\left[\frac{Z - 4/N}{2^{4/3}N^{-5/3}}\right]. \tag{103}$$

This shows that $\lambda_{\max}$ in our problem typically fluctuates on a scale $O(N^{-5/3})$ around its average $4/N$,

$$\text{typical } \lambda_{\max} = \frac{4}{N} + 2^{4/3}N^{-5/3}\chi_\beta, \tag{104}$$

where the distribution of the random variable χ_β is the Tracy-Widom probability density function $g_\beta(x) = dF_\beta(x)/dx$. Around the mean value we have then

$$P\left(\lambda_{\max} = \frac{t}{N}\right) \approx N^{5/3} g_\beta(2^{-4/3}N^{2/3}(t - 4)). \tag{105}$$

Matching Between the Tails of the Tracy-Widom Distribution and the Large Deviation Rate Functions For Gaussian and Wishart matrices, it has been recently demonstrated [33–36] that the Tracy-Widom density describing the probability of typical fluctuations of the largest eigenvalue matches smoothly, near its tails, with the left and right rate functions that describe the probability of atypical large fluctuations. It would be interesting to see if the same matching happens in our problem as well. Indeed, we find that the tails of the Tracy-Widom distribution match smoothly to our previously obtained rate functions.

For the left tail of the Tracy-Widom density, it is known [51, 52] that $g_\beta(x) \sim \exp\{-\frac{\beta}{24}|x|^3\}$ for $x \to -\infty$. Therefore $P(\lambda_{\max} = \frac{t}{N}) \sim \exp\{-\beta N^2 \frac{|t-4|^3}{384}\}$. On the other hand, for the rate function to the left of the mean describing large fluctuations of $\sim O(1/N)$ is given in (92). Taking the limit $t \to 4^-$, we find $\chi_{II}(t) \approx -\frac{(t-4)^3}{384}$ thus matching smoothly with the left tail of the Tracy-Widom density.

For the right tail, one knows [51, 52] $g_\beta(x) \sim \exp\{-\frac{2\beta}{3}x^{3/2}\}$ for $x \to +\infty$. Therefore $P(\lambda_{\max} = \frac{t}{N}) \sim \exp\{-\beta N \frac{(t-4)^{3/2}}{6}\}$. On the other hand, the rate function describing large fluctuations of order $\sim O(1/N)$ to the right of the mean is given in (93). Expanding to leading order for $t \to 4^+$, we get: $\chi_{III}(t) \approx \frac{(t-4)^{3/2}}{6}$ which clearly matches smoothly to the right tail of the Tracy-Widom density.

6 Numerical Simulations

To verify the analytical predictions derived in the preceding sections, we simulated the joint distribution of eigenvalues in (5):

$$P(\lambda_1, \ldots, \lambda_N) = B_{M,N} \delta\left(\sum_i \lambda_i - 1\right) \prod_{i=1}^{N} \lambda_i^{\frac{\beta}{2}(M-N+1)-1} \prod_{i<j} |\lambda_i - \lambda_j|^\beta$$

$$= B_{M,N}\, \delta\!\left(\sum_i \lambda_i - 1\right) e^{-\beta E[\{\lambda_i\}]}, \tag{106}$$

where the effective energy $E[\lambda_i]$ is given by $E[\lambda_i] = -\gamma \sum_{i=1}^{N} \ln \lambda_i - \sum_{i<j} \ln|\lambda_i - \lambda_j|$ with $\gamma = \frac{M-N+1}{2} - \frac{1}{\beta}$ and with $\sum_i \lambda_i = 1$. We sampled this probability distribution using a Monte Carlo Metropolis algorithm (see [53]).

6.1 Standard Metropolis Algorithm

We start with an initial configuration of the λ_i's satisfying $\sum_{i=1}^{N} \lambda_i = 1$ and $\lambda_i > 0$ for all i. At each step, a small modification $\{\lambda_i\} \to \{\lambda_i'\}$ is proposed in the configuration space. In our algorithm, the proposed move consists of picking at random a pair (λ_j, λ_k) (with $j \neq k$) and proposing to modify them as $(\lambda_j, \lambda_k) \to (\lambda_j + \epsilon, \lambda_k - \epsilon)$, which naturally conserves the sum of the eigenvalues. ϵ is a real number drawn from a Gaussian distribution with mean zero and with a variance that is set to achieve an average rejection rate $1/2$.

The move is rejected if one of the eigenvalues becomes negative. Otherwise, the move is accepted with the standard probability

$$p = \min\!\left(\frac{P(\lambda_1', \ldots, \lambda_N')}{P(\lambda_1, \ldots, \lambda_N)}, 1\right) = \min\!\left(e^{-\beta(E[\{\lambda_i'\}]-E[\{\lambda_i\}])}, 1\right), \tag{107}$$

and rejected with probability $1 - p$. This dynamics enforces detailed balance and ensures that at long times the algorithm reaches thermal equilibrium (at inverse "temperature" β) with the correct Boltzmann weight $e^{-\beta E[\{\lambda_i\}]}$ and with $\sum_i \lambda_i = 1$.

At long times (from about 10^6 steps in our case), the Metropolis algorithm thus generates samples of $\{\lambda_i\}$ drawn from the joint distribution in (106). We can then start to compute some functions of the λ_i's, e.g. the purity $\Sigma_2 = \sum_i \lambda_i^2$, and construct histograms, e.g. for the density, the purity, etc.

However, as the distribution of the purity (as well as the one of the eigenvalues) is highly peaked around its average, a standard Metropolis algorithm does not allow to explore in a "reasonable" time a wide range of values of the purity. The probability to reach a value $\Sigma_2 = s/N$ decreases rapidly with N as $e^{-\beta N^2 \Phi(s)}$ where $\Phi(s)$ is a positive constant (for s different from the mean value: $s \neq \bar{s}$). Therefore, we modified the algorithm in order to explore the full distribution of the purity and to compare it with our analytical predictions.

6.2 Method 1: Conditional Probabilities

It is difficult to reach large values $\Sigma_2 = s/N$ of the purity ($s > \bar{s}$). The idea is thus to force the algorithm to explore the region $s \geq s_c$ for different values of s_c. We thus add in the algorithm the constraint $s \geq s_c$. More precisely, we start with an initial configuration that, in addition to $\sum_i \lambda_i = 1$ and $\lambda_i > 0$ for all i, satisfies also $\sum_i \lambda_i^2 \geq s_c/N$. At each step, the proposed move is rejected if $\sum_i \lambda_i'^2 < s_c/N$. If $\sum_i \lambda_i'^2 \geq s_c/N$, then the move is accepted or rejected exactly with the same Metropolis rules as before. Because of the new constraint $s \geq s_c$, the moves are rejected much more often than before. Therefore the variance of the Gaussian distribution $P(\epsilon)$ has to be taken smaller to achieve a rejection rate $1/2$.

We run the program for several values of s_c (about 20 different values) and we construct a histogram of the purity for each value s_c. This gives the conditional probability distribution $P(\Sigma_2 = \frac{s}{N} | \Sigma_2 \geq \frac{s_c}{N})$. Again, as the distribution of the purity is highly peaked, the algorithm can only explore a very small range of values of s—even for a large running time (about

10^8 steps). The difference with the previous algorithm is that we can now explore small regions of the form $s_c \leq s \leq s_c + \eta$ for every s_c, whereas before we could only explore the neighbourhood of the mean value $\bar{s}$.

The distribution of the purity is given by

$$P\left(\Sigma_2 = \frac{s}{N}\right) = P\left(\Sigma_2 = \frac{s}{N} \Big| \Sigma_2 \geq \frac{s_c}{N}\right) * P\left(\Sigma_2 \geq \frac{s_c}{N}\right) \quad \text{(for } s_c < s). \tag{108}$$

Therefore the rate function reads:

$$\Phi(s) = -\frac{1}{\beta N^2} \ln P\left(\Sigma_2 = \frac{s}{N}\right)$$

$$= -\frac{1}{\beta N^2}\left[\ln P\left(\Sigma_2 = \frac{s}{N} \Big| \Sigma_2 \geq \frac{s_c}{N}\right) + \ln P\left(\Sigma_2 \geq \frac{s_c}{N}\right)\right]. \tag{109}$$

The histogram constructed by the algorithm with the constraint $s \geq s_c$ is the rate function $\Phi_{s_c}(s) = -\frac{1}{\beta N^2} \ln P(\Sigma_2 = \frac{s}{N} | \Sigma_2 \geq \frac{s_c}{N})$. $\Phi_{s_c}(s)$ differs from the exact rate function $\Phi(s)$ by an additive constant that depends on s_c. In order to get rid of this constant, we construct from the histogram giving $\Phi_{s_c}(s)$ the derivative $\frac{d\Phi_{s_c}(s)}{ds}$. This derivative is equal to $\frac{d\Phi(s)}{ds}$ and the constants disappear. We can now compare numerical data with the derivative of the analytical expression for the rate function $\Phi(s)$.

We can also come back to $\Phi(s)$ from its derivative using an interpolation of the data for the derivative and a numerical integration of the interpolation. This allows to compare directly the numerical results with the theoretical rate function $\Phi(s)$.

We can follow the same steps to explore the region on the left of the mean value $s < \bar{s}$ by adding in the simulations the condition $\sum_i \lambda_i^2 \leq \frac{s_c}{N}$ (instead of $\sum_i \lambda_i^2 \geq \frac{s_c}{N}$) for several values of $s_c < \bar{s}$.

We typically run the simulations for $N = 50$ and 10^8 iterations. As Fig. 5 shows, numerical data and analytical predictions agree very well for regimes **I** and **II** (rate functions given in (32) and (36)). For regime **III**, finite-size effects are important and agreement holds for large but finite N analytical formulae (taking as rate function the expression of the energy in (55) with t and ζ numerical solutions of the system of equations (53) and (54)). The agreement would degrade for the asymptotic rate function giving only the dominant term for very large N (45). Finite-size effects are also important for the transition between regimes **II** and **III**. Large-N data are crucial to see clearly this abrupt transition with a sudden jump of the maximal eigenvalue. For $N = 50$, the transition appears indeed to be smoothed out. This observation can be rationalized as follows. At the transition ($s = s_2$), the maximal eigenvalue t is expected to jump for large N from a value $\sim \frac{5}{N}$ to a much larger value $\sim \sqrt{\frac{s-2}{N}}$, yet for $N = 50$ we have $\frac{5}{N} > \sqrt{\frac{s-2}{N}}$ for all $s < 9/4$. We thus conclude that no jump can be seen at $N = 50$ and much larger N are needed. Adapting the simulation method to cope with this challenge is the subject of the next subsection.

6.3 Method 2: Simulation of the Density of Eigenvalues (and Conditional Probabilities)

We want to be able to run simulation for very large values of N. The idea is to simulate the density $\rho(\lambda) = \frac{1}{N} \sum_i \delta(\lambda - \lambda_i)$ rather than the eigenvalues themselves. In the previous scheme, a configuration was made of N variables, the N eigenvalues. In the new code, we have $k + 2 \ll N$ variables:

(1) the maximal eigenvalue t.
(2) the upper bound of the density support ζ ($\zeta < t$).
(3) the value of the density at each point $x_i = \frac{i\zeta}{k}$ (for $0 \leq i < k$).

We must enforce the condition $\rho(\zeta) = 0$, i.e. $\rho(x_k) = 0$ by definition of the upper bound ζ of the density support. The idea is to replace the real density by a linear approximation of the density defined by its value at x_i for $0 \leq i \leq k$.

These $k + 2$ variables describing the maximal eigenvalue and the density of the other eigenvalues simulate configurations with $N \gg k$ eigenvalues, for example $N = 1000$ with $k = 50$. The number of eigenvalues N appears in the expression of the energy (and in the constraints). With this new code, we can now simulate configurations with many eigenvalues in a reasonable time.

6.3.0.1 The Algorithm From the analytical calculations, we expect that the density diverges when $\lambda \to 0^+$ as $\rho(\lambda) \sim \frac{1}{\sqrt{\lambda}}$. In order to get a better approximation in our code, we choose to discretize a regularized form of the density $\bar{\rho}(\lambda) \equiv \sqrt{\lambda}\rho(\lambda)$. Our $(k + 2)$ variables are thus:

(1) the maximal eigenvalue t.
(2) the upper bound of the regularized density support ζ ($\zeta < t$), which is the same as the upper bound of the density support.
(3) the value of the regularized density at each point $x_i = \frac{i\zeta}{k}$ (for $0 \leq i < k$): $z_i \equiv \bar{\rho}(x_i)$.

In the Monte Carlo simulation, we compute the energy as well as the constraints ($\sum_i \lambda_i = 1$, etc.) by using a linear interpolation of the regularized density $\bar{\rho}(\lambda)$:

$$\tilde{\rho}(\lambda) = z_i + \frac{z_{i+1} - z_i}{x_{i+1} - x_i} (\lambda - x_i) \quad \text{for } \lambda \in [x_i, x_{i+1}[, \tag{110}$$

with $z_i = \bar{\rho}(x_i)$ (in particular $z_k = 0$). Integrals such as $\int d\lambda \, \lambda \, \rho(\lambda)$ are computed using the linear interpolation as:

$$\int_0^\zeta d\lambda \rho(\lambda)\lambda \approx \frac{4}{15} \left(\frac{\zeta}{k}\right)^{\frac{3}{2}} \left[z_0 + \sum_{i=1}^{k-1} z_i \{(i+1)^{\frac{5}{2}} + (i-1)^{\frac{5}{2}} - 2i^{\frac{5}{2}}\}\right]. \tag{111}$$

There are two constraints for the density : the normalization $\int \rho = 1$ and the unit sum of the eigenvalues $t + (N - 1) \int \lambda\rho = 1$. We start from an initial configuration satisfying these constraints: for example, we can take for the initial ρ a density of the form of the (normalized) average density $\rho(\lambda) = \frac{2}{\pi\zeta}\sqrt{\frac{\zeta-\lambda}{\lambda}}$ and fix t with the unit sum constraint $t = -(N - 1) \int \lambda\rho + 1$. Initially, we also choose ζ not too large such that the condition $\sum_i \lambda_i^2 > s_c/N$ is satisfied (for a fixed value of s_c), exactly as in the code with conditional probabilities.

At each step, we propose a move in the configuration space (our $k + 2$ variables) that naturally enforces the two constraints $\int \rho = 1$ and $t + (N - 1) \int \lambda\rho = 1$ (unit sum). More precisely, at each step we choose randomly three integers between 0 and $k+1$: $i_1 < i_2 < i_3$.

– If $i_3 < k$ (case 1), we propose a move $(z_{i_1}, z_{i_2}, z_{i_3}) \to (z_{i1} + \alpha_1\epsilon, z_{i2} + \alpha_2\epsilon, z_{i3} + \alpha_3\epsilon)$, where ϵ is drawn from a Gaussian distribution with zero mean and a variance adjusted to have the standard rejection rate $1/2$ at the end. α_1, α_2 and α_3 are constants that are chosen such that the constraints $\int \rho = 1$ and $t + (N - 1) \int \lambda\rho = 1$ (unit sum of eigenvalues) are

satisfied:

$$\alpha_1 = \left[(i_3+1)^{3/2} + (i_3-1)^{3/2} - 2i_3^{3/2}\right]\left[(i_2+1)^{5/2} + (i_2-1)^{5/2} - 2i_2^{5/2}\right]$$
$$- \left[(i_2+1)^{3/2} + (i_2-1)^{3/2} - 2i_2^{3/2}\right]\left[(i_3+1)^{5/2} + (i_3-1)^{5/2} - 2i_3^{5/2}\right]$$

α_2 and α_3 are obtained from α_1 by cyclic permutation of i_1, i_2 and i_3.

- If $i_1 < i_2 < i_3 = k$ (case 2), we propose a move $(\zeta, z_{i_1}, z_{i_2}) \rightarrow (\zeta + \epsilon, z_{i1} + \epsilon_1, z_{i2} + \epsilon_2)$ where ϵ is drawn from a Gaussian distribution with zero mean and a variance adjusted to have the standard rejection rate $1/2$ at the end (different from the variance of case 1), and where ϵ_1 and ϵ_2 are functions of ϵ, i_1 and i_2 fixed by the two constraints ($\int \rho = 1$ and unit sum).
- If $i_1 < i_2 < k$ and $i_3 = k + 1$ (case 3), we propose a move $(t, z_{i_1}, z_{i_2}) \rightarrow (t + \epsilon, z_{i1} + \epsilon_1, z_{i2} + \epsilon_2)$, where, exactly as in case 2, ϵ is drawn from a Gaussian distribution, and ϵ_1 and ϵ_2 are functions of ϵ, i_1 and i_2 fixed by the two constraints ($\int \rho = 1$ and unit sum).
- If $i_1 < i_2 = k$ and $i_3 = k + 1$ (case 4), we propose a move $(\zeta, z_{i_1}, t) \rightarrow (\zeta + \epsilon, z_{i1} + \epsilon_1, t + dt)$, where ϵ is drawn from a Gaussian distribution (same as in case 2), and ϵ_1 and dt are functions of ϵ and i_1 fixed by the two constraints ($\int \rho = 1$ and unit sum).

Then, if $\zeta > t$, if $\zeta < 0$, if $z_i < 0$ or if $\sum_i \lambda_i^2 < s_c/N$, that is $(N-1)\int \lambda^2 \rho + t^2 < s_c/N$, the move is rejected. Otherwise we compute the energy of the new configuration E_{new} and accept the move with the usual Metropolis probability $p = \min(e^{-\beta(E_{\text{new}}-E)}, 1)$ (and reject it with probability $1 - p$).

Direct inspection of the previous rules shows that detailed balance is satisfied. Therefore, after a large number of iterations, thermal equilibrium with the appropriate Boltzmann weight is reached and we can start to construct histograms of the density and the purity. We verified that for $N = 50$ (simulated with $k + 2$ variables, where $k = 20$) we recover the results of the direct Monte Carlo (where we simulate directly the eigenvalues). For $N = 500$ and $N = 1000$ (with $k = 50$), we get very interesting results that can be used to test the large-N analytical predictions (see (32) and (36) for regimes **I** and **II** and (45) for regime **III**): Fig. 6 shows the good agreement between theory and numerical simulations with this second method, for the distribution of the purity $\Sigma_2 = \sum_i \lambda_i^2$ with $N = 1000$. As Fig. 7 shows, we can really see the abrupt jump of the maximal eigenvalue and the change of behaviour of the rate function (discontinuous derivative), which is expected at the transition between regime **II** and regime **III** for very large N.

The simulations also provide solid support to the fact that a single eigenvalue detaches from the sea in regime III. One might indeed wonder whether configurations with multiple charges detaching from the sea could be more favorable. This was ruled out by measuring the area of the rightmost "bump" in the density of charges (see Fig. 3) and verifying that it corresponds to a single charge. This fact is also intuitively rationalized as follows. Let us consider configurations with two charges, λ_1 and λ_2 ($\lambda_1 \geq \lambda_2$), detaching from the sea. As in (47), we require $\lambda_1^q + \lambda_2^q = t^q$ and we consider the quantity $\mathcal{C} = 1 - \lambda_1 - \lambda_2$, which quantifies the compression of the sea of charges and would replace $1 - t$ in the μ_1 constraint in (47). The smaller is $\mathcal{C}$, the stronger is the compression of the sea (with the other constraints remaining the same). Since the charges repel each other, the energy of the configuration is expected to increase as $\mathcal{C}$ gets smaller. An elementary calculation shows that, due to the convexity of λ^q for $q > 1$, $\mathcal{C}$ is minimum when $\lambda_1 = \lambda_2 = 2^{-1/q}t$ while its maximum (minimum energy) is attained at the boundary $\lambda_1 = t$, $\lambda_2 = 0$, corresponding indeed to a single charge detaching from the sea.

7 Conclusion

In this paper, by using a Coulomb gas method, we have computed the distribution of the Renyi entropy S_q for $q > 1$ for a random pure state in a large bipartite quantum system, i.e. with a large dimension N of the smaller subsystem. We have showed that there are three regimes in the distribution $P(S_q = \ln N - z)$ that are a direct consequence of two phase transitions in the associated Coulomb gas.

(i) Regime **I** corresponds to the left tail of the distribution ($0 < z < z_1(q)$). In this phase, the effective potential seen by the Coulomb charges has a minimum at a nonzero point. The charge density has a finite support over $[L_1, L_2]$ (and vanishes at L_1 and L_2), the charges accumulate around the minimum of the potential.

(ii) Regime **II** describes the central part of the distribution ($z_1(q) < z < z_2(q)$), and in particular the vicinity of the mean value $\bar{z}(q)$. At the transition between regimes **I** and **II**, the third derivative of the rate function (logarithm of the distribution) is discontinuous. In this phase, the charges concentrate around the origin, the charge density has a finite support over $[0, L]$ with a square-root divergence at the origin. Close to the mean value of S_q, the distribution is Gaussian.

(iii) Regime **III** describes the right tail of the distribution ($z > z_2(q)$), corresponding to a more and more unentangled state. In this phase, one charge splits off the sea of the other charges. The transition between regimes **II** and **III** is abrupt with a sudden jump of the rightmost charge (largest eigenvalue). There is thus a discontinuity of the derivative of the rate function (first-order phase transition) and the scaling with N changes at this point.

A by-product of our results is the fact that, although the average entropy is close to its maximal value $\ln N$, the probability of a maximally entangled state is actually very small. The probability density function of the entropy indeed vanishes at $z = 0$ (far left tail), i.e. at $S_q = \ln N$, which is the maximally entangled situation. Similar properties and three different regimes are also obtained in the limit $q \to 1$, which gives us the distribution of the von Neumann entropy, and in the limit $q \to \infty$, which yields the distribution of the maximal eigenvalue.

References

1. Nielsen, M.A., Chuang, I.L.: Quantum Computation and Quantum Information. Cambridge University Press, Cambridge (2000)
2. Lubkin, E.: J. Math. Phys. (N.Y.) **19**, 1028 (1978)
3. Lloyd, S., Pagels, H.: Ann. Phys. (N.Y.) **188**, 186 (1988)
4. Page, D.N.: Phys. Rev. Lett. **71**, 1291 (1993)
5. Hall, M.J.W.: Phys. Lett. A **242**, 123 (1998)
6. Bohigas, O., Giannoni, M.J., Schmit, C.: Phys. Rev. Lett. **52**, 1 (1984)
7. Bandyopadhyay, J.N., Lakshminarayan, A.: Phys. Rev. Lett. **89**, 060402 (2002) and references therein
8. Giraud, O., Martin, J., Georgeot, B.: Phys. Rev. A **79**, 032308 (2009)
9. Vidal, G.: J. Mod. Opt. **47**, 355 (2000)
10. Facchi, P., Florio, G., Pascazio, S.: Phys. Rev. A **74**, 042331 (2006)
11. Facchi, P., Florio, G., Parisi, G., Pascazio, S.: Phys. Rev. A **77**, 060304(R) (2008)
12. Facchi, P., Marzolino, U., Parisi, G., Pascazio, S., Scardicchio, A.: Phys. Rev. Lett. **101**, 050502 (2008)
13. Zyczkowski, K., Sommers, H.-J.: J. Phys. A, Math. Gen. **34**, 7111–7125 (2001)
14. Cappellini, V., Sommers, H.-J., Zyczkowski, K.: Phys. Rev. A **74**, 062322 (2006)
15. Giraud, O.: J. Phys. A, Math. Theor. **40**, 2793 (2007)
16. Znidaric, M.: J. Phys. A, Math. Theor. **40**, F105 (2007)
17. Majumdar, S.N., Bohigas, O., Lakshminarayan, A.: J. Stat. Phys. **131**, 33 (2008)

18. Majumdar, S.N.: Extreme eigenvalues of Wishart matrices: application to entangled bipartite system. In: Akemann, G., Baik, J., Di Francesco P. (eds.) Handbook of Random Matrix Theory. Oxford University Press, London (2010, to appear). arXiv:1005.4515
19. Chen, Y., Liu, D.-Z., Zhou, D.-S.: arXiv:1002.3975
20. Nadal, C., Majumdar, S.N., Vergassola, M.: Phys. Rev. Lett. **104**, 110501 (2010)
21. De Pasquale, A., Facchi, P., Parisi, G., Pascazio, S., Scardicchio, A.: Phys. Rev. A **81**, 052324 (2010)
22. James, A.T.: Ann. Math. Stat. **35**, 475 (1964)
23. Akemann, G., Cicutta, G.N., Molinari, L., Vernizzi, G.: Phys. Rev. E **59**, 1489 (1999)
24. Akemann, G., Cicutta, G.N., Molinari, L., Vernizzi, G.: Phys. Rev. E **60**, 5287 (1999)
25. Lakshminarayan, A., Tomsovic, S., Bohigas, O., Majumdar, S.N.: Phys. Rev. Lett. **100**, 044103 (2008)
26. Foong, S.K., Kanno, S.: Phys. Rev. Lett. **72**, 1148–1151 (1994)
27. Sánchex-Ruiz, J.: Phys. Rev. E **52**, 5653 (1995)
28. Sen, S.: Phys. Rev. Lett. **77**, 1 (1996)
29. Sommers, H.-J., Zyczkowski, K.: J. Phys. A, Math. Theor. **37**, 8457 (2004)
30. Kubotini, H., Adachi, S., Toda, M.: Phys. Rev. Lett. **100**, 240501 (2008)
31. Vivo, P.: arXiv:1006.0088
32. Forrester, P.J.: Log-Gases and Random Matrices. Princeton University Press, Princeton (2010). http://www.ms.unimelb.edu.au/matpjf/matpjf.html
33. Dean, D.S., Majumdar, S.N.: Phys. Rev. Lett. **97**, 160201 (2006)
34. Dean, D.S., Majumdar, S.N.: Phys. Rev. E **77**, 041108 (2008)
35. Vivo, P., Majumdar, S.N., Bohigas, O.: J. Phys. A, Math. Theor. **40**, 4317 (2007)
36. Majumdar, S.N., Vergassola, M.: Phys. Rev. Lett. **102**, 060601 (2009)
37. Katzav, E., Castillo, I.P.: arXiv:1005.5058
38. Nadal, C., Majumdar, S.N.: Phys. Rev. E **79**, 061117 (2009)
39. Vivo, P., Majumdar, S.N., Bohigas, O.: Phys. Rev. Lett. **101**, 216809 (2008)
40. Vivo, P., Majumdar, S.N., Bohigas, O.: Phys. Rev. B **81**, 104202 (2010)
41. Kazakopoulos, P., Mertikopoulos, P., Moustakasa, A.L., Caire, G.: arXiv:0907.5024 (2009)
42. Bray, A.J., Dean, D.S.: Phys. Rev. Lett. **98**, 150201 (2007)
43. Fyodorov, Y.V., Williams, I.: J. Stat. Phys. **129**, 1081 (2007)
44. Majumdar, S.N., Nadal, C., Scardicchio, A., Vivo, P.: Phys. Rev. Lett. **103**, 220603 (2009)
45. Tricomi, F.G.: Integral Equations. Pure Appl. Math., vol. V. Interscience, London (1957)
46. Marčenko, V.A., Pastur, L.A.: Math. USSR Sb. **1**, 457 (1967)
47. Majumdar, S.N., Evans, M.R., Zia, R.K.P.: Phys. Rev. Lett. **94**, 180601 (2005)
48. Evans, M.R., Majumdar, S.N., Zia, R.K.P.: J. Stat. Phys. **123**, 357 (2006)
49. Johansson, K.: Commun. Math. Phys. **209**, 437 (2000)
50. Johnstone, I.M.: Ann. Stat. **29**, 295 (2001)
51. Tracy, C., Widom, H.: Commun. Math. Phys. **159**, 151 (1994)
52. Tracy, C., Widom, H.: Commun. Math. Phys. **177**, 727 (1996)
53. Krauth, W.: Statistical Mechanics: Algorithms and Computation. Oxford University Press, Oxford (2006)